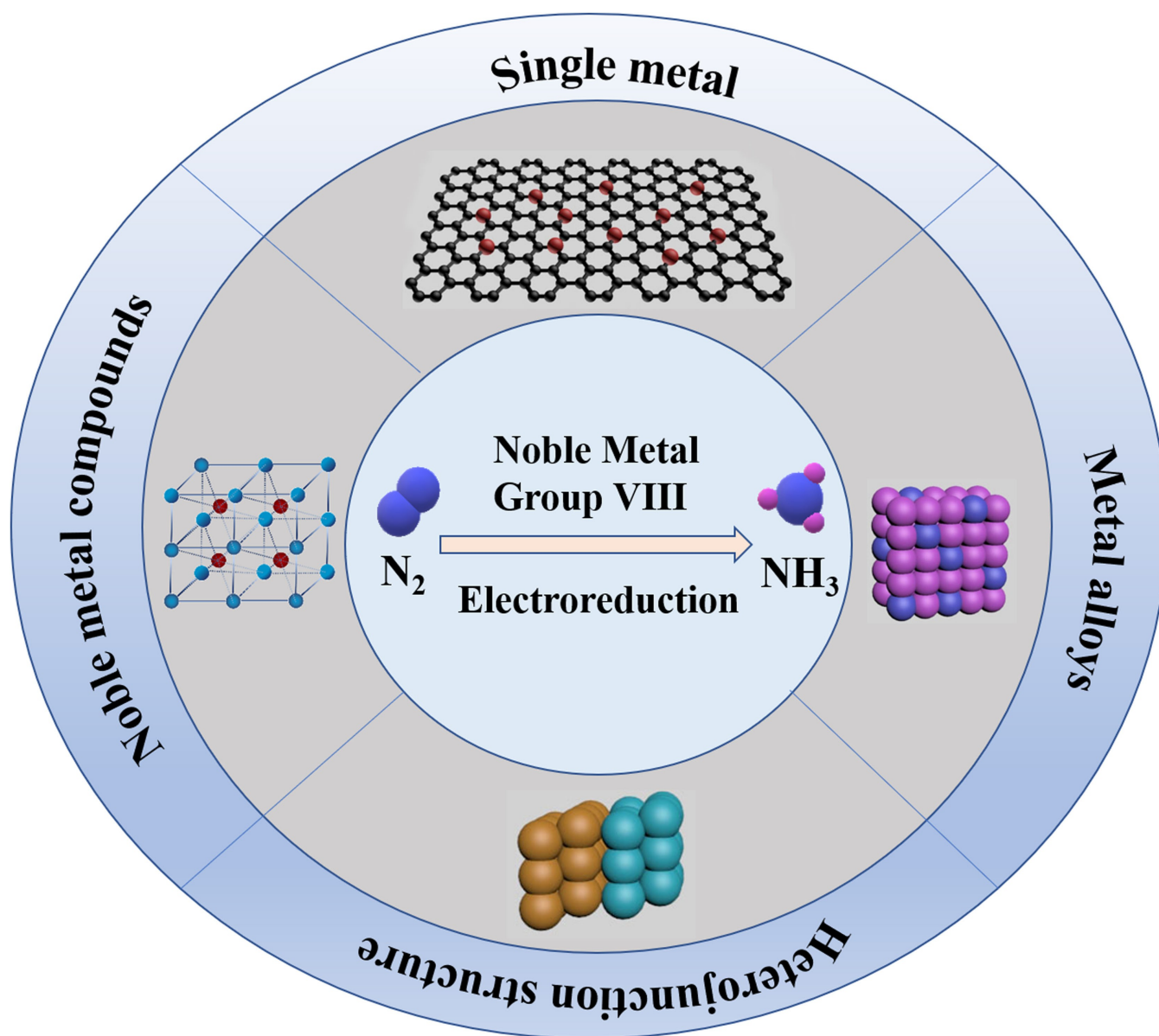Special Collection

An Overview on Noble Metal (Group VIII)-based Heterogeneous Electrocatalysts for Nitrogen Reduction Reaction

Qianqian Chen[+], Xiaodong Zhang[+], Yuwei Jin, Xuemei Zhou,* Zhi Yang,* and Huagui Nie*[a]

Abstract: The typically the Haber-Bosch process of nitrogen (N₂) reduction to ammonia (NH₃) production, expends a lot of energy, resulting in severe environmental issues. Electrocatalytic N₂ reduction to NH₃ formation by renewable resources is one of the effective ways to settle the issue. However, the electro-catalytic performances and selectivity of catalysts for electrochemical nitrogen reduction reaction (NRR) are very low. Therefore, it is of great significance to develop more efficient electro-catalysts to satisfy the needs of practical use. Among the reported catalysts, those based on Group VIII noble metals heterogeneous catalysts display excellent NRR activities and high selectivity because of their good conductivity, rich active surface area, unfilled d-orbitals, and the abilities with easy adsorption of reactants and stable reaction intermediates. Herein, we will introduce the progress of Group VIII precious metals heterogeneous catalysts applied in the electrocatalytic N₂ reduction reaction. Then single precious metal electrocatalysts, precious metal alloy electrocatalysts, heterojunction structure electrocatalysts, and precious metal compounds based on the strategies of morphology engineering, crystal facet engineering, defect engineering, heteroatom doping, and synergetic interface engineering will be discussed. Finally, the challenges and prospects of the NH₃ synthesis have been put forward. In the review, we will provide helpful direction to the development of effective electro-catalysts for catalytic N₂ reduction reaction.

1. Introduction

Nitrogen (N) is a fundamental element in many biological processes. Nevertheless, biological fixation of nitrogen (N₂) in the nature is difficult to satisfy the sharp increase in needs of agricultural industries that can ensure the supply of grain for population growth.[1] Despite the volume of N₂ in the atmosphere is over 78%, it is very difficult to use N₂ owing to the stable property of N≡N triple bond. Ammonia (NH₃) is the primary product of N₂ reduction, and it is the raw materials for the synthesis of chemical fertilizer, and also the ideal storage media for hydrogen (H₂) with high hydrogen content (17.65%). At present, the synthesis of ammonia is mainly via the Haber-Bosch method for reducing N₂ to NH₃ ($N_2 + 3H_2 \leftrightarrow 2NH_3$) in ammonia plants based on coal or natural gas. Nevertheless, the Haber-Bosch process has some drawbacks: the cost of clean hydrogen generated from the fossil fuels is high; the energy consumption and greenhouse gas emissions are huge; the NH₃ yield (conversion rates of 10%–15% from N₂) is usually low, and the reaction conditions are harsh (400–500 °C, >60 bar).[1c,2] Thus, it is greatly important to develop alternative methods for efficient synthesis of NH₃ under mild reaction conditions.

Lately, some facile methods for NRR have been proved, such as the use of biological nitrogenase and photocatalytic and electrocatalytic methods.[3] Biological fixation of nitrogen is generated by the nitrogenase at normal temperature and pressure; but nitrogenases are sensitive to oxygen. Photocatalytic N₂ reduction is not as efficient as that of electrocatalysis, which is due to rapid carrier recombination produced by multiple wavelengths light in the process of photocatalysis, and thus not all of them can be utilized. It is possible to adopt electrochemical reduction method on a heterogeneous surface at normal temperatures and pressures as long as enough voltage is used. Electro-catalytic NRR is considered to be the most promising method to NH₃ synthesis by virtue of its advantages of environmental friendliness, low energy consumption, renewable solar and wind-driven energy.

To date, great research efforts have been made to the development of electro-catalysts for high efficiency of NRR under ambient conditions.[2c,3–4] Homogeneous electro-catalysts are usually molecular complexes including transition metals, which are first dissolution in acid medium and reduced on the surface of the electrode, meanwhile the electrode itself is inert to NRR. Heterogeneous catalysts are generally applied to overcome the drawbacks of homogeneous catalysts. Heterogeneous catalysts are usually formed by different geometric and chemical structures of metals or metal-based solids. Since heterogeneous electro-catalysis take place between the electrode and electrolyte interface, their surface properties and the structure information have an important effect on determining their catalytic performance. Therefore, there is a strategy to increase the heterogeneous catalysts of inherent activities. For instance, theoretical and experimental plans combined with the regulation of the crystal, defects, electronic structure, or morphology structures of the catalysts, can boost the chemical adsorption of N₂ molecules and reveal more catalytic active sites, and thus improving NRR catalytic activities of NRR.[5] Another tactics is to devise the appropriate catalysts or special reaction system to restrain the competitive hydrogen evolution reaction (HER). For instance, the solubility of N₂ in the solution can be improved by adjusting the electrolytes.[6] Recently, researches are increasing interest in electrochemical NRR at normal temperatures and pressures. With rapid advancement of different analytical tools and technologies, several upscale instruments that can provide *in-situ* and microtest analyses are now available. These techniques will offer more deeper messages on the real NRR processes, and help us direct observation of the electro-catalytic process and accurate analysis of the mechanisms of NRR.

Among heterogeneous catalysts, those based on Group VIII noble metals display excellent NRR activities and high selectivity

[a] Q. Chen,+ X. Zhang,+ Y. Jin, X. Zhou, Z. Yang, H. Nie
Key Laboratory of Carbon Materials of Zhejiang Province, College of Chemistry and Materials Engineering, Wenzhou University, Wenzhou, 325027 (P. R. China)
E-mail: zxm.mei@163.com
yang201079@126.com
huaguinie@126.com
[+] These authors contributed equally to this work.
This manuscript is part of a special collection on Defect Chemistry.

because of their good conductivity, rich active surface area, unfilled d-orbitals, and the abilities with easy adsorption of reactants and stable reaction intermediates.[7] Specifically, the electrons of N_2 can be synergistically accepted with appropriate energy and symmetry, which is attributed to the unoccupied and occupied d orbitals of noble metals (Group VIII). N atoms in N_2 molecules can offer lone-pair electrons to unoccupied d orbitals in the noble metals (Group VIII) through the sp hybridization of N atoms. The occupied d orbitals in the metals can donate electrons in reverse to the π-molecular orbitals of the dinitrogen.[8] This process reduces the N≡N bond and strengthens the bond of metal-nitrogen. Herein, we mainly present recent progress in the use of noble metal (VIII)-based electrocatalysts for NRR at normal temperatures and pressures. This paper first introduces the basic concepts of the electrochemical NRR. Then, we give a summary of noble metal (group VIII)-based catalytic systems by dividing them into single precious metal electrocatalysts, noble metal alloy electrocatalysts, heterojunction structure electrocatalysts, and precious metal compounds, which are designed based on the strategies of morphology engineering, crystal facet engineering, defect engineering, heteroatom doping, and electrode-catalyst-electrolyte interface engineering. The relationships between optimal electro-catalytic conditions and the performance of NH_3 production are emphasized in this paper, which provides a prospect for the researchers to carry out the high efficient electrocatalysts for NH_3 synthesis. In the review, we provide practical guidance to design and develop high efficient electrocatalysts with high Faradaic efficiency (FE) and NH_3 yield.

2. Basic understanding of NRR

The reaction process is the core of any chemical reactions, in which the molecules of the reactants are changed into serviceable products.[3] The catalyst plays an important role in accelerating the conversion process, resulting in a highly efficient chemical reaction process. It requires an understanding of the basic chemical reactions in order to successfully develop chemical reaction processes. Herein, some elementary concepts

Qianqian Chen is currently a postgraduate student at Key Laboratory of Carbon Materials of Zhejiang Province, College of Chemistry and Materials Engineering, Wenzhou University, P. R. China. Her research topic is the synthesis of heterogeneous catalyst materials and their application for electrocatalytic ammonia synthesis.

Xiaodong Zhang is currently a postgraduate student at Key Laboratory of Carbon Materials of Zhejiang Province, College of Chemistry and Materials Engineering, Wenzhou University, P. R. China. His research interests focus on nanomaterials-based electrocatalysis including nitrogen reduction reaction and hydrogen evolution reaction.

Yuwei Jin is currently a postgraduate student at Key Laboratory of Carbon Materials of Zhejiang Province, College of Chemistry and Materials Engineering, Wenzhou University, P. R. China. His research topics include nanomaterials synthesis and their application in water splitting such as oxygen evolution reaction.

Xuemei Zhou received her Ph.D. from the Center for Applied Chemical Research, Frontier Institute of Science and Technology, Xi'an Jiaotong University, in 2017. Then, she worked as a postdoc (2017–2019) in School of Material and Energy, Guangdong University of Technology. Now, she fully works at Key Laboratory of Carbon Materials of Zhejiang Province, College of Chemistry and Materials Engineering, Wenzhou University. Her research interests include nanomaterials design for catalysis and energy conversion/storage applications.

Zhi Yang earned a Ph.D. from College of Materials Science and Engineering, Hunan University, in 2009. He is currently a full Professor at Key Laboratory of Carbon Materials of Zhejiang Province, College of Chemistry and Materials Engineering, Wenzhou University. His research interests cover the preparation of nanomaterials and their applications in fuel cell and lithium-sulfur battery.

Huagui Nie earned a Ph.D. from State Key Laboratory of Chemo/Biosensing and Chemometrics, Hunan University, in 2009. She is currently a full Professor at Key Laboratory of Carbon Materials of Zhejiang Province, College of Chemistry and Materials Engineering, Wenzhou University, P. R. China. Her research interests include biosensors, electrocatalysis, and fuel cell based on functionalized nanomaterials.

of the electrochemical NRR are discussed, containing the reactions on the cathode and anode, mechanisms of NRR, evaluation criteria and experimental methods of catalytic performances.

2.1. NRR reactions occurring on cathodes and anodes

Electro-catalysis NRR is one of the most promising methods to produce ammonia under conditions of normal temperature and pressure. As one of the main raw materials, H_2O is oxidized at the anode, while NRR occurs at the cathode. The overall reaction process can be presented as:

$$N_2 + 3H_2O \rightarrow 1.5O_2 + 2NH_3$$
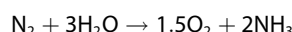
However, the reaction process is different in different electrolyte solutions. In acidic medium, protons produced by the anodes can be directly shifted to the cathode through proton exchange membrane, leading to the NH_3 formation. Equations (1) and (2) show the two half-reactions for anodic side and cathodic side under acidic conditions.[3]
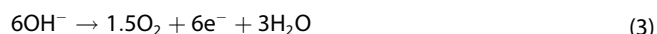
Oxidation reaction at anodic side

$$3H_2O \rightarrow 6H^+ + 1.5O_2 + 6e^- \tag{1}$$

Reduction reaction at cathodic side

$$6H^+ + N_2 + 6e^- \rightarrow 2NH_3 \tag{2}$$

In an alkaline environment, N_2 acquires electrons and combines with H_2O, and reacts on the cathode to form NH_3 and OH^-. The OH^- ions via the anion exchange membrane transferred to the anode and then oxy-generated. Equations (3) and (4) represent the two electrode reactions.[3]
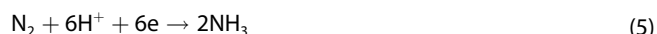
Oxidation reaction at anodic side

$$6OH^- \rightarrow 1.5O_2 + 6e^- + 3H_2O \tag{3}$$

Reduction reaction at cathodic side

$$6H_2O + N_2 + 6e^- \rightarrow 2NH_3 + 6OH^- \tag{4}$$

In the neutral condition, the water is also oxidized to generate O_2 and protons (H^+). The protons produced by the anode are transported through the conductive separated membrane to the cathode side filled with N_2 gas, resulting in NH_3 formation:

$$N_2 + 6H^+ + 6e \rightarrow 2NH_3 \tag{5}$$

2.2. Criteria for efficient NRR electrocatalysts

Improving electrochemical NRR performance of catalysts is the kernel to boost the evolution of this territory, and thus it is especially significant to objectively and accurately evaluate their performance. Generally speaking, the NH_3 yield rate, FE, and cyclic stability are considered as the significant indexes for evaluating the NRR catalysts performance.[9] An effective NRR catalyst should be able to activate N_2 to form NH_3 at a low overpotential with minimal by-products, such as H_2, N_2H_2, and N_2H_4. It should also retain catalytic activities and selectivity for a long lifetime.

The yield of the product and the FEs can be calculated from formulas (6)-(9):[9]

$$r_{NH3} = (17cNH_3 \times V)/(t \times m) \tag{6}$$

$$r_{N2H4} = (c_{N2H4} \times V)/(t \times m) \tag{7}$$

$$FE_{NH3} \ (\%) = (3F \times cNH_3 \times V)/Q \tag{8}$$

$$FE_{N2H4} \ (\%) = (4F \times cNH_3 \times V)/Q \tag{9}$$

In which F: the Faraday constant, c: the measured concentration of NH_3 or N_2H_4, V: the electrolyte solution volume, t: the reduction time, m: the mass of the electrocatalyst, and Q: the total charge in the reduction process. There will be some adjustments depending on the units.

2.3. Experimental methods for NRR

2.3.1. Rigorous conduct of experiments

Ammonia molecules are widespread in the environment, and will be found in the laboratory and its equipment, such as gloves, reaction devices, gas supplies, and experimental reagents. As pointed out by Wang and Qiao, the use of standard experimental procedures makes experimental data more credible.[1a,c] Therefore, use of acid or alkali solution as an ammonia trap is likely to improve the accuracy of experimental results. Catalysts, electrolytes, and reagents must be prepared and purified in earlier experiments to ensure that ammonia production cannot take place in the inert argon atmosphere. Bare electrodes must be tested in Ar-saturated electrolyte solutions at open circuit voltage and working voltage, which can eliminate pollution of the experimental equipment and can eliminate the pollution of catalysts during ammonia production. In addition, the isotopic tracer method can be used to prove the sources of nitrogen. The specific schematic diagram of the measurements to conduct the NRR experiments is shown in Figure 1.

2.3.2. Choice of electrolyte

Electrolyte solution plays one of the most important roles in the electro-catalysis process.[10] Aqueous electrolytes, including phosphate buffer solution (PBS),[11] H_2SO_4,[11] KOH,[11] $HClO_4$,[12] HCl,[13] Na_2SO_4,[14] and Li_2SO_4[4d,15] have been widely used in NRR system where temperature is often maintained from room
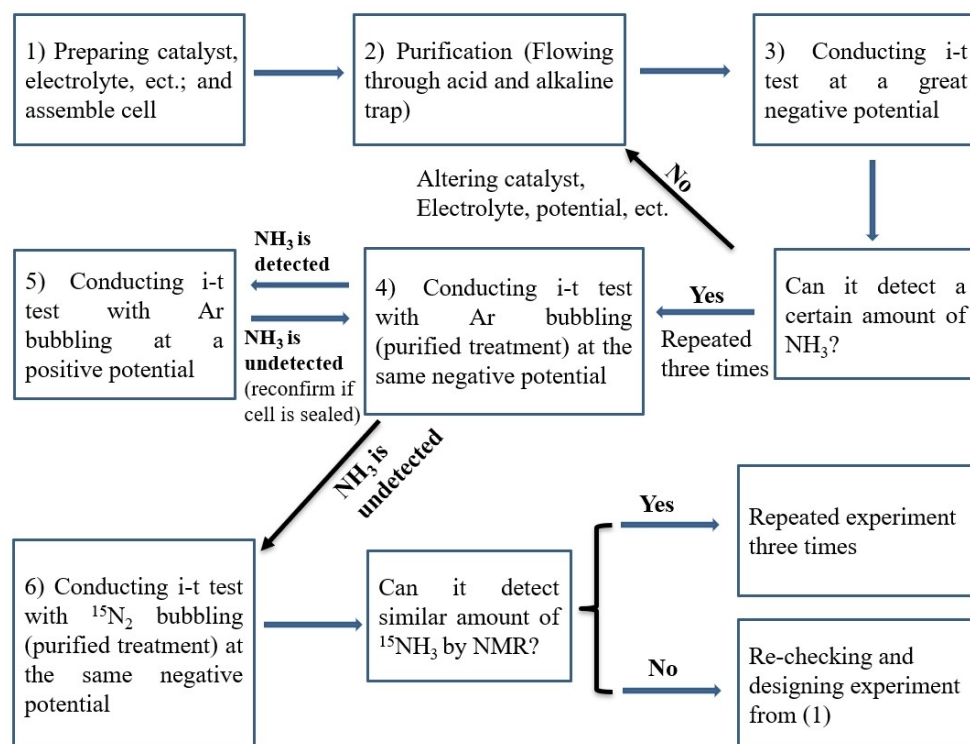
Figure 1. The specific schematic diagram of the measurements is to conduct the NRR experiments. The i-t refers to the chronoamperometric technique.

temperature to 60 °C to avoid significant water evaporation. NRR,[4b] HER,[16] and oxygen evolution reaction (OER)[17] take place only in aqueous electrolytes and the parameters are easy to adjust, such as pH and the ions type and concentration. However, high concentration of water and low solubility of N_2 are still the main issue to limit NRR catalytic performance. Moreover, it is difficult to resolve the suppression of HER and mass transfer of N_2 in aqueous electrolytes, limiting the FE of electro-catalysts. Based on several theoretical studies, non-aqueous electrolyte has the advantages of high nitrogen solubility, low water content and significant inhibition of HER, making it an ideal choice for NRR research. However, the formation rate of ammonia in non-aqueous electrolytes is much lower than that in other electrolytes, which is possibly caused by poor protons mass transfer. Additionally, the overpotential of NRR in non-aqueous electrolytes is usually high because the ionic conductivities are poor. Furthermore, all working electrodes used in non-aqueous electrolytes display similar structures composed of catalysts grown on conductive carriers (such as

carbon fiber, nickel foam, et. al), which is difficult to determine the loading of electrocatalysts. Ion conducting membranes, such as proton exchange membranes and anion exchange membranes, can be applied in the electrochemical NRR at room temperature (RT). Benefiting from the advantages of these membranes with the low thickness and high ionic conductivity, the NRR systems show the relatively low resistance, making fast ammonia formation rates. However, the FEs of NRR using anion exchange membranes was much lower than that of the aqueous electrolytes, because it is difficult to adjust the parameters of the membranes. The advantages and disadvantages of different electrolytes are listed in Table 1. Therefore, the design and development of novel electrolytes may make the greater progress for high effective electrochemical N_2 reduction with low overpotentials, fast NH_3 formation rates and high FEs at the appropriate temperature, which it is believed as a more vigorous pursuit for the researchers.

Table 1. The properties and application conditions of various electrolytes.

Electrolytes	T [°C]	Merits	Demerits
Aqueous electrolytes	RT-60	Easy to adjust parameters including pH, the concentration of the ions, the types of cations and anions	High water concentration; low N_2 solubility; competition of HER
Non-aqueous electrolytes	RT	High N_2 solubility; a low water content; inhibition of HER	Poor ionic conductivity and protons mass transfer; high NRR overpotentials; difficult to determine the loading of electrocatalysts
Ion-conductive membranes	RT-200	Low resistance; fast ammonia formation rates	Low FEs; difficult to adjust the parameters of the membranes

2.3.3. Reaction equipment

At present, the catalytic activities of NRR catalysts are usually assessed by adopting electrochemical workstations with three electrode systems. Various electrochemical cells have been developed using liquid electrolyte or solid electrolyte. According to recent experimental investigations, the electrochemical reactors can be grouped into four types according to different cell structures, as given in Figure 2.

Amar et al.,[19] Kyriakou et al.,[4a] and Zhang et al.[18] have reviewed the merits and drawbacks of four categories of reactors, summarized in Table 2. For example, the back-to-back cell with the positive and negative electrodes parted by a tight membrane is suitable for solid-state electrochemical ammonia

synthesis over a wide temperature range. Nafion films could be used the separated membrane due to their high proton conductivity at ambient temperature; however, the proton conductivity of them was lowered due to a lacks of water, reducing the NH_3 yield. Unlike proton exchange membranes, anion exchange membranes (AEM) selectively transfer hydroxyl anions to the anode, making the alkaline environment of cells more superior. In addition to solid-state electrolyte, liquid electrolyte can be also used in back-to-back cell, which expands the selection of the catalyst and electrolyte. When compared with the conventional solid-state polymer membrane cell, polymer electrolyte membrane (PEM)-type cells have two advantages: adding a reference electrode (RE) is convenient to measure the working electrode (WE) potential, and fully wet the
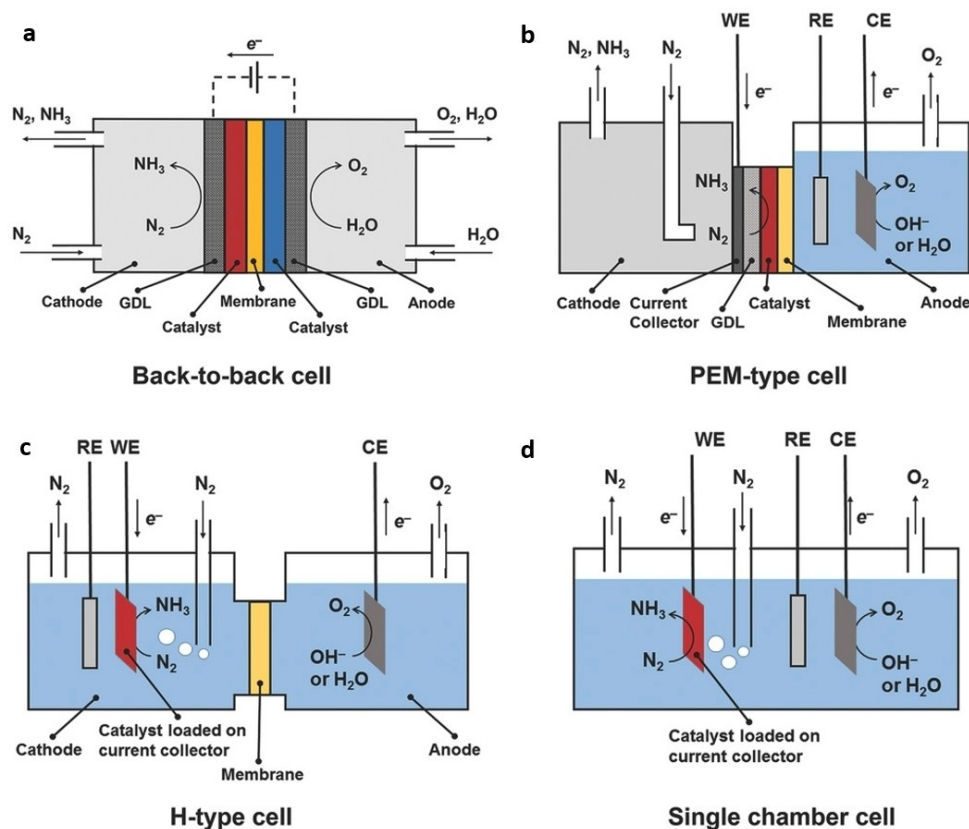

Figure 2. a–d) Schematic diagrams of various cell equipment for electro-catalytic NRR. Copyright 2018 Wiley-VCH.[18]

Table 2. The strengths and weaknesses of each cell type.		
Cell types	Advantages	Disadvantages
back-to-back cell	(1) It is suitable for solid-state electrochemical ammonia synthesis over a wide temperature range. (2) The back-to-back type cell can also enable the use of liquid electrolyte, which extends the selection of catalysts and electrolytes.	The proton conductivity of the separated membranes (Nafion) was lowered due to a lacks of water, reducing the NH_3 yield.
PEM-type cell	(1) The convenience of adding a reference electrode enables the measurement of the potential of the working electrode; (2) The adequate wetting of the membrane reduces the conductivity loss of the membrane.	It suffers from the ammonia crossover effect.
H-type cell	Both the working electrode and the reference electrode are located in the cathode chamber, making it more accurate to measure the applied potentials, exerted on the working electrode.	The H-type cell with Nafion membrane as the separator exhibits ammonia/ammonium crossover effect.
single-chamber cell	It is simple and easy to operate.	Gaseous products at the anode may be oxidized at the anode.

film to compensate the loss of the film conductivity. In the H-type cell, both the WE and RE are placed in the negative side, which makes measurement of the potentials applied to the WE more accurate than in the PEM-type cell, where the RE must be located in the positive side full of electrolyte. However, the H-type cell separated by Nafion film also displays ammonia/ammonium crossover effects similar to those of PEM-type cells. Thus, it is recommended to use both the cathode and anode electrolytes to measure the total production of ammonia. Additionally, a membrane or an additional anti-diffusion layer should be used to prevent ammonia cross effect to a great extent. As for the single chamber cell, it is simple and easy to operate. But there is a drawback of the single-chamber cell with three electrodes in the same chamber, because the generated products on the positive electrode may be easily oxy-generated. Thus this experimental configuration is rarely used.

Given that the electro-catalytic NRR experimental systems are complicated, some factors probably have an influence on NH$_3$ synthesis. These include cell reactors, the catalysts on the electrodes and the electrolyte properties. To accurately evaluate the performance of NRR electro-catalysts, a suitable reactor should be selected and the above factors should be optimized.

2.3.4. Appropriate electrochemical techniques

The availability of suitable electrochemical techniques (cyclic voltammetry (CV), linear scanning voltammetry (LSV), chronopotentiometric (CP) and chronoamperometric (CA) methods) to monitor nitrogen reduction is the key to quantitative determination of ammonia and the calculation of FE.[1a,c]

The electrochemical behavior of NRR across a potential range is usually characterized by the LSV technique. By analyzing the differences of the current densities of LSV results with Ar and N$_2$, we can decide whether or not the catalyst has catalytic activity for NRR. It is not recommended to use LSV, CV and CP techniques to measure the FEs of NRR, because the potential of these techniques is different during the catalytic reaction time, which is not conducive to controlling the equilibrium between NRR and HER. In most of the reports, the values of FEs are calculated by the CA data, because we can be accurate control of the applied voltages and well investigate the effect between the potentials and the FEs. Based on a set of CA measurements at given applied voltages, the maximum FEs can be obtained at an optimal potential.

In some cases, electrochemical impedance spectroscopy (EIS) can also be used to measure the electron conductivity property of catalysts and to understand the catalytic kinetics for NRR. The series resistance (Rs) and the resistance of charge transfer (Rct) can be obtained from the Nyquist diagrams, which often are referred to the resistance of electrolyte solution and charge transfer in the catalyst, respectively.[20] Some special porosity resistance (Rp) can be also obtained based on some literatures by the equivalent circuit. However, the matched equivalent circuit is of subjectivity, which may not accurately represent the reality, and is also disputable.

The relationships of NRR activities and electrocatalytically active surface area (ECSA) have been demonstrated by several literatures.[1a,c,21] The ECSA of electrocatalysts can be generally calculated by measuring the capacitance by CV in the non-Faradaic region.[6] Notably, Pt-based catalysts of ECSA can be determined via the H adsorption-desorption from CV curves.[22] Pd-based catalysts of ECSA can be calculated by the reduction charge of PdO reduction peak from CV curves.[21b] Although each catalyst with different preparation method, catalyst loadings and morphology, will lead to different catalytic ability of NRR in the previous reports, the electrochemical results (the current densities, NH$_3$ yield rates) can be normalized to the ECSA to exclude the effects of different catalysts, allowing for a fair comparison. In a word, to obtain more helpful and credible results, the above-mentioned electrochemical measurements should be repeated several times under near-identical conditions during the whole experiments.

2.3.5. Detection of ammonia

Ion chromatography and colorimetric methods based on Nessler's reagent or indophenols-blue colorimetry are typically used for NH$_3$ detection. Ion chromatography is a kind of high-efficiency liquid chromatography, also known as high-efficiency ion chromatography or modern ion chromatography, which uses conductivity as the detection technique. It has the merits of high sensibility and good recurrence, but it needs expensive equipment and instruments. The method using Nessler's reagent has the advantages of a wide range of electrolyte pH applicability and high accuracy. However, the service lifetime of Nessler's reagent is short (about 3 weeks), and water for preparing the reagent must be free of ammonia (ultra-pure water). The indophenol blue method is commonly used for ammonia detection in NRR. It has high accuracy for solutions with low NH$_3$ content, tolerates a wide pH range, and is easy to perform. Notably, the deionized water still contains a certain amount of ammonia. Strong acid cation exchange resin can play an effective role in purifying the ammonia in the deionized water. The cation exchange resin was pretreated by water washing (washing until drainage colorless and no bubble). Then the resin was soaked in the NaOH solutions (2%–4%) for 5–6 hours, cleaning with water to pH = 7–9. After that, hydrochloric acid solution (5%) was poured in the resin and kept for 6 hours. The acid solution was drained and rinsed with water until neutral. Lastly, a certain amount of deionized water was put into the resin at 60 °C. After about 48 hours, the ammonia content in the water was significantly reduced. For gas purification, the gas was washed twice by 1 M sulfuric acid, and the purified gas could be collected as the raw material for electrocatalytic reduction. By the above treatment, the impact of ammonia in the environment would be minimized. Additionally, at least two or more methods should be selected according to the specific needs to ensure accuracy of the data in the actual operation.

2.3.6. Detection of $^{15}NH_4^+$

Isotope tracing is one of the important measurements used to explore NRR. Such heterogeneous catalytic systems can be affected by many factors, including the presence of N_2 molecules on the catalyst surface, the adsorption and activation modes, the microchemical environment of the active site, and the external environment. Therefore, it is highly recommended to use isotopically labeled $^{15}N_2$ to confirm the formation of $^{15}NH_3$ via direct N_2 fixation, and to detect product ($^{15}NH_4^+$) by ^1H nuclear magnetic resonance (NMR) spectroscopy, because the peak area of the ^1H NMR and the concentration of NH_3 exhibit a linear relation. The yields of NH_3 can be calculated from the ^1H NMR spectrum of 15NH^{4+}, which requires to be identified with the results from other detection methods. Aside from ^1H NMR spectroscopy, Fourier transform infrared spectroscopy and mass spectrometry can also be applied in qualitative detection of ^{15}N-labeled NH_3.[23] Thus, the researchers should be pay more attention to the actual NH_3 formation in the future work, which should be obtained via the different ammonia detection methods and combine with the isotope tracing experiment to make it convincing.

2.4. Mechanisms of NRR

Molecular nitrogen is composed of two N≡N triple bonds and each N atom has five valence electrons outside its inner shell, arranged in the configuration $2s^22p^3$. As observed from Figure 2a, it exists four bonding orbitals and four anti-bonding orbitals in the hybridized N_2 molecule.[24] Activation of N_2 requires overcoming a large gap of 10.82 eV within the highest occupied molecular orbital (HOMO) and the lowest unoccupied molecular orbital (LUMO), and the molecule has a large ionization energy (15.58 eV). The essential issues of the electrochemical N_2 reduction to NH_3 will be studied from the thermodynamic limitations applied to the reaction intermediates. Therefore, the reactions of various NRR in different electrolytes are given in Table 3:[18] As observed from Table 3, it is found that except for the difficult activation of nitrogen (R5 and R9), the electrolytes of electro-catalytic NRR is also along with a strong competitive side effects (by-products, the formation of hydrogen), since the standard balance potential of NRR is very close to that of HER (R1 vs R2, R3 vs R4). Moreover,

electrochemical pathway of NRR may be transferred through a coupled or sequential proton-electron process (R5-R8), and the schematic illustration is given in Figure 3b. As a result, the current development of NRR is more limited than might be expected.

To date, the mechanisms of nitrogen reduction have been mainly divided into three types: dissociative, associative, and enzymatic pathways (Figure 3c–e).[1a,c,8–9,18,25] The N≡N bond is fully broken prior to any hydrogenation process, leaving a single N adsorption atom to hydrogenate and further change into NH_3 in the dissociation mechanism. NRR in the conventional Haber-Bosch method abides by the dissociation mechanism, and the fracture of the N≡N bond is attributed to high internal energy. Thus, the mechanism of dissociation path is unfavorable to NRR at normal temperature and pressure.

By contrast, the N≡N bond in the association path is incompletely broken until the first NH_3 releases. According to different hydrogenation sequences, there are distal process, the alternating process and enzymatic process in the association pathways. In the distal paths, the hydrogenation first happens on the distal N atom far from the surface. When the N atom is delivered in the form of NH_3, another remote N atom is hydrogenated into another molecule of NH_3. In the alternating process, the two N atoms go through single hydrogenation in turn. In the enzymatic process, the process of the hydrogenation happens successively on the two N atoms with the side-on adsorption modes.

In addition to the above mechanisms, Abghoui and Skúlason has also put forward a Mars-van Krevelen (MvK) mechanism used in the NRR process at the transition metal nitride (TMN)-based catalysts surface.[26] Based on the mechanism, ammonia molecules are generated by reducing the nitrogen atoms on the catalyst surface, and then the produced N vacancies are supplemented by the nitrogen, thus achieving a continuous reaction. The MvK mechanism is more thermodynamic advantageous in breaking the N≡N bond than those of the traditional dissociation and association mechanisms. In addition, some transition metal nitrides and transition metal complexes may also have federated reaction mechanisms accompanied by association and dissociation pathways as well as the MvK mechanism.

3. NRR on noble metal (VIII) catalysts

Considering that structures, morphologies, compositions, and defects are the primary influences on the catalytic activities of heterogeneous catalysts, many strategies have been applied to develop and design of high efficient electro-catalysts for NRR.[1c,2a,c,3,4d,5a] According to the NRR mechanism, an active center with an easy adsorption N_2 molecules and weakness the N≡N bond is of great importance for the formation and activation of N_2. Density functional theory (DFT) is a significant tool to detect catalytic active sites of NRR and offer theoretical direction to seek for optimal electro-catalysts. For instance, DFT has been widely used on transition metal surfaces in acidic medium at room temperature and pressure for dissociative and

Table 3. The reactions of various NRR products.

$N_2 + 6H^+ + 6e^- \rightleftharpoons 2NH_3$ (g), $E^0 = +055$ V vs NHE	R1
$6H^+ + 6e^- \rightleftharpoons H_2$ (g), $E^0 = 0$ V vs SHE at pH = 0	R2
$N_2 + 6H_2O + 6e^- \rightleftharpoons 2NH_3$ (g) + 6OH$^-$, $E^0 = -0.736$ V vs SHE at pH = 14	R3
$2H_2O + 2e^- \rightleftharpoons H_2$ (g) + 2OH$^-$, $E^0 = -0.828$ V vs SHE at pH = 14	R4
$N_2 + H^+ + e^- \rightleftharpoons N_2H$, $E^0 = -3.2$ V vs RHE	R5
$N_2 + 2H^+ + 2e^- \rightleftharpoons N_2H_2$, $E^0 = -1.1$ V vs RHE	R6
$N_2 + 4H^+ + 4e^- \rightleftharpoons N_2H_4$, $E^0 = -0.36$ V vs RHE	R7
$N_2 + 4H_2O + 6e^- \rightleftharpoons N_2H_4$ (g) + 4OH$^-$, $E^0 = -1.16$ V vs SHE at pH = 14	R8
$N_2 + e^- \rightleftharpoons N_2^-$ (aq), $E^0 = -3.37$ V vs RHE at pH = 14	R9

Note: NHE: normal hydrogen electrode, SHE: standard hydrogen electrode, and RHE: reversible hydrogen electrode.
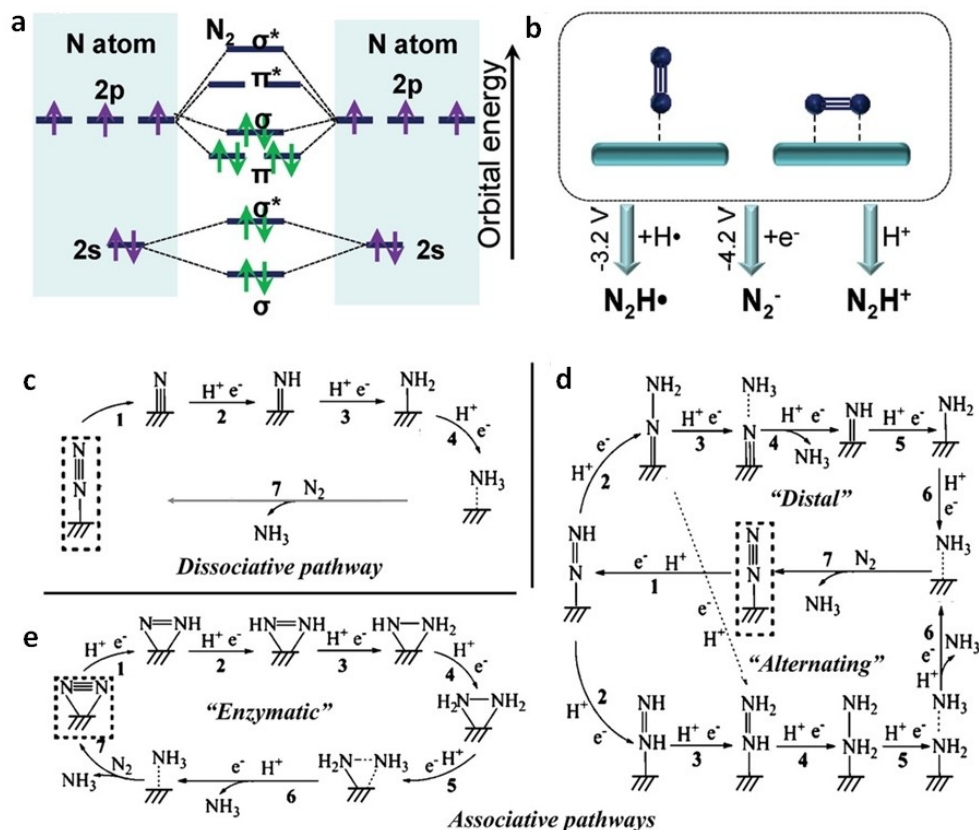
Figure 3. a) Molecular orbital illustration of N_2. b) The schematic diagram of coupled or sequential proton-electron transfer processes. Copyright 2020 Wiley-VCH.[24] c–e) Schematic depiction of the mechanisms of NRR. Copyright 2018 Wiley-VCH.[18]

associative pathways of NRR (Figure 4a).[5c] The electrons of N_2 can be synergistically accepted with appropriate energy and symmetry because of the nature of precious metals unoccupied and occupied d orbitals. N atoms in N_2 molecules can offer lone-pair electrons to unoccupied d orbitals in the noble metals (Group VIII) through the sp hybridization of N atoms. Meanwhile, the occupied d orbits in the metals can donate electrons in reverse to the π-molecular orbitals of the N_2 molecules, making the N≡N bond is fragile and strengthening the metal-

nitrogen bond (Figure 4b).[27] Precious metals have been widely used as catalysts for various electrochemical reactions, due to their good conductivity and high binding abilities to many reactants.[28] In recent years, the precious metals are also used as electro-catalysts for NH_3 synthesis at normal temperature and pressure. The extensively applied precious metals for NRR are ruthenium (Ru), rhodium (Rh), palladium (Pd), and platinum (Pt).[7a,11,29]
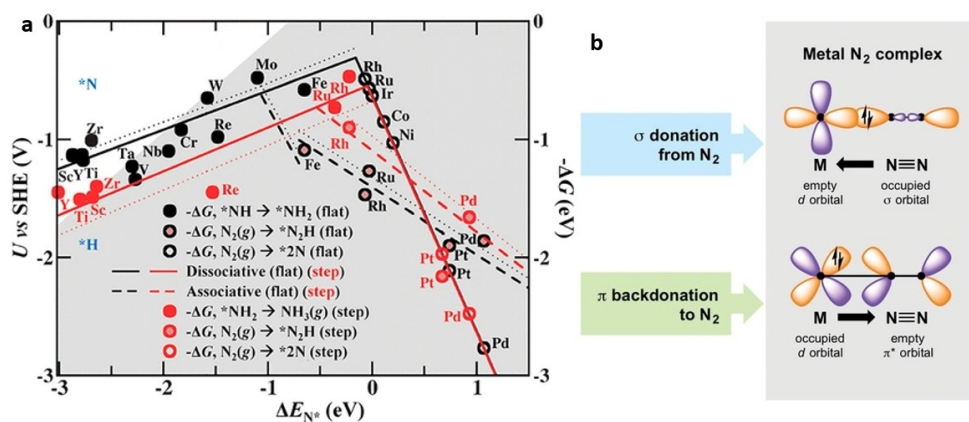

Figure 4. a) The pathways of dissociation (solid line) and association (dotted line) on the metal surfaces. Copyright 2012 the PCCP Owner Societies.[5c] b) The type of bonding in transition-metal N_2 complexes. Copyright 2018 American Association for the Advancement of Science.[27]

3.1. Single-metal electrocatalysts for NRR

Ru and Rh located at the top of NRR's the theoretical volcano map, have drawn a lot interests from scientists and have been extensively used as catalysts for NRRs.[29c] Ruthenium was electrodeposited on carbon felt as NRR electro-catalysts in solid polymer electrolyte (SPE) cells under environmental conditions.[7a] The Ru-based SPE cell generated NH_3 yield ($0.21 \times 10^{-6} \, g \, cm^{-2} \, h^{-1}$) and FE of 0.28%, at 1.10 V. There was no detection of hydrazine (N_2H_4, by-product of NRR) during the reaction, indicating the formation of NH_3 was by the dissociative mechanism on the electrodeposited Ru. This work was pointed out that the main restrictions of the Ru-based cell were low NH_3 production rates and current efficiency. Similar issues were also observed from Rh electro-catalysts by electrochemical deposition method.[1b,29c]

To improve NRR performance, some strategies were developed for Ru and Rh electrocatalysts. Zeng designed Ru single-atom dispersed on N-doped carbon (Ru SAs/N—C) catalysts via decomposition of zeolitic imidazolate frameworks (ZIF-8) consisted of Ru (Figure 5a).[7b] The authors demonstrated that Ru atoms with a valence of approximately +3 in the Ru SAs/N—C catalysts because it was coordinated by N atoms, compared with the bonds of Ru—Ru metallic in Ru nanoparticles supported on N-doped carbon (Ru NPs/N—C). The Ru SAs/N—C catalysts exhibited FEs of 29.6% and NH_3 yield rates of $120.9 \, \mu g_{NH3} \, mg_{cat}^{-1} \, h^{-1}$ in the acid medium, much larger than that of Ru NPs/N—C electro-catalysts at the same conditions (Figure 5h-**5i**), which could be attributed that the Ru SAs/N—C catalyst had much stronger binding of N_2 than that of the Ru NPs/N—C catalyst based on the N_2-TPD (temperature-programmed desorption) results. According to DFT analysis, the authors came to a conclusion that Ru SAs/N—C facilitated the N_2 adsorption, and the ΔG value for N_2 dissociation on Ru SAs/N—C is smaller than that on Ru (101), which resulted in enhanced of

NRR activity. The Ru SAS/N—C catalysts also exhibited analogical FEs in the neutral and alkaline solutions, making that it could be used in all pH conditions. However, both NH_3 yield rates and FEs decreased with increased more negative potentials (Figure 5h–5i), which caused by the competitive reaction of HER. Notably, the determination of ammonia is produced by electrochemical NRR through a series of control experiments and also used the isotope trace method. Qiao and co-workers have also demonstrated that a graphite carbon nitride-supported 20 different monatomic transition metal (TM) ($TM@g-C_3N_4$) electrocatalysts displayed high activities for electrochemical NRR in strong basic medium under mild conditions.[30] The limiting potentials of these TM-SAs were evaluated by DFT computations and the reaction mechanism was displayed by analyzing their electronic structures. It concluded that the limiting potentials of these systems were as a function of the N* adsorption energy of (ΔE_{N*}) (Figure 6a and **6b**). In addition, the change of ΔE_{N*} was caused by the effect of metal centers on the bonding/antibonding orbital distributions. Another reports via DFT calculations also demonstrated that the reaction Ru $SAs/g-C_3N_4$ was thermodynamically more favorable than that of bulk Ru surfaces, improving the NRR activities of Ru SAs/ $g-C_3N_4$.[7c]

The surfactant-free ultra-thin Rh nanosheet (RhNN) (about 1 nm) as an efficient electrocatalyst for NRR under ambient conditions was prepared by Liu et al. (Figure 7).[31] This catalyst displayed high efficient catalytic performance with the NH_3 yield of $23.88 \, \mu g \, h^{-1} \, mg_{cat}^{-1}$, which was attributed to high speci surface area and outstanding electronic structures of the nanosheet (Figure 7J). Meanwhile, RhNN also showed good selectivity and long lifetime for NRR in an alkalic solution. Three-dimensional (3D) nanostructures allow fast ion/molecule transport and provide a huge area of exposed active sites.[32] Thus, it is important to establish 3D Rh particulate catalysts that also act in this way for NRR. Recently, 3D Rh particles were
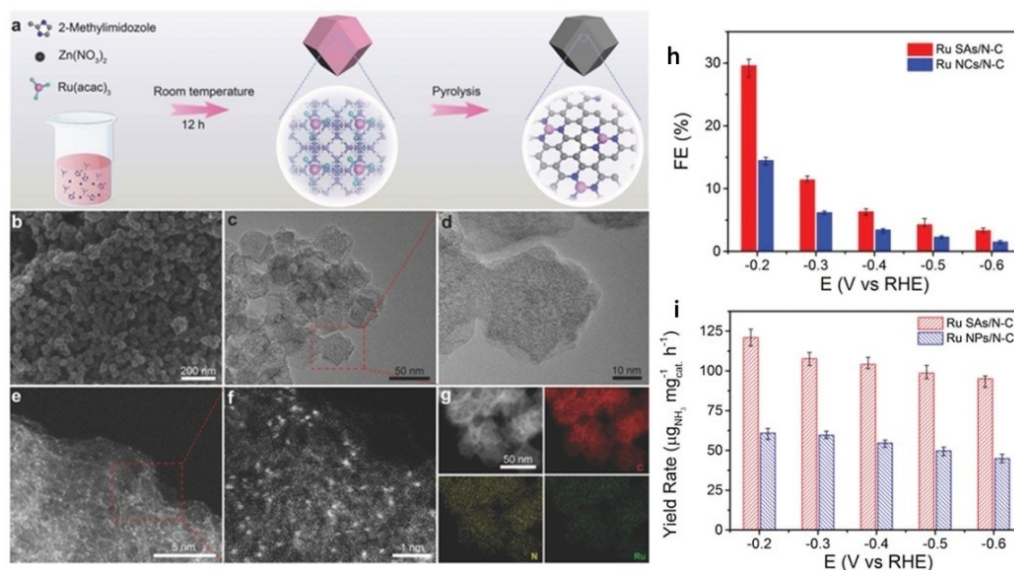

Figure 5. a) Schematic diagram of Ru SAs/N—C synthesis; b–g) the characterization of Ru SAs/N—C; Ru SAs/N—C and Ru NPs/N—C of FE (h) and NH_3 yield (i). Copyright 2018 Wiley-VCH.[7b]
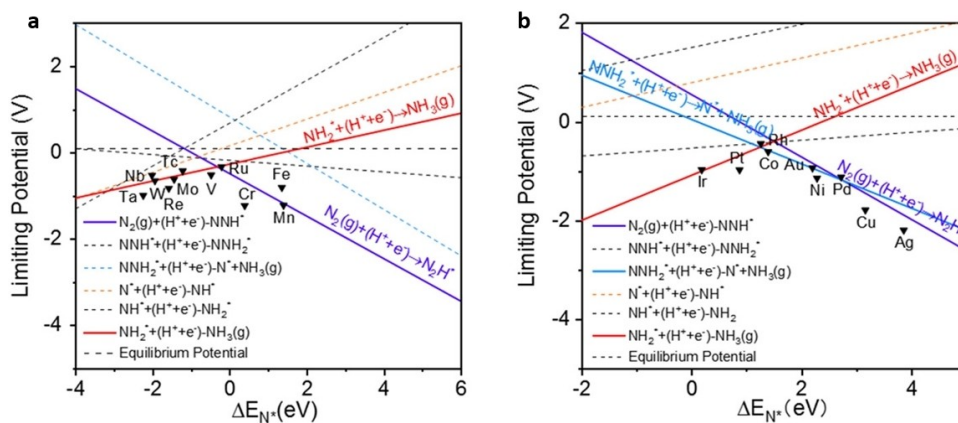
Figure 6. The transition metal systems of limiting potential defined as a function of the adsorption energy of *N (ΔE_{N^*}) for the early transition metal a) and late transition metal b). Copyright 2019 American Chemical Society.[30]
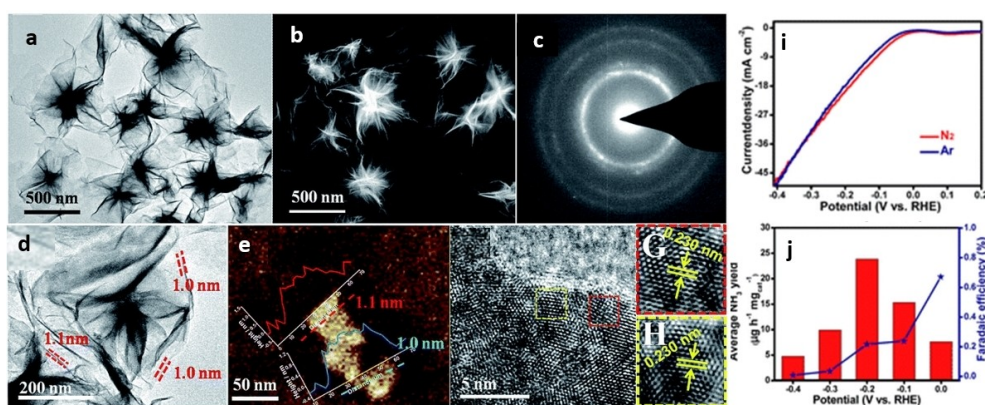

Figure 7. a–h) The characterization of Rh NNs; i–j) The electrocatalytic performance curves of Rh NNs. Copyright 2019 The Royal Society of Chemistry.[31]

prepared in a one-step method using the ionic liquid,[29a] which acted as reductants, structural-guiding agents, and reaction media for the growth of the 3D Rh particles. The as-grown 3D Rh particulate catalysts proved long time of stability and good selectivity for NRR. This strategy using ionic liquids offers more chances to design advanced NRR catalysts.

To further study the mechanism of NRR on noble metal surfaces, some operando characterization tools have been used. For example, Yao et al. conducted NRR in acidic solution to go deep into understanding the Ru catalysts of NRR mechanism by applying strong surface-enhanced infrared absorption spectroscopy (SEIRAS).[33] N_2 was adsorbed on a clean surface at the applied positive voltage by cycling from $+0.4$ to -0.4 V, and then the hydrogenations of N_2 were tested by monitoring a band range from 1850 to 1995 cm^{-1} (Figure 8a), which was caused by N≡N stretching. The relationship between the position of N≡N stretching and the potential of CV was given in Figure 8**b**, it could be concluded that when the potential decreased from 0 to -0.15 V, the band strength significantly increased, indicating that the coverage area of *N_2H_x absorption increased. In addition, only the Ru–H stretching was detected in the Ar-saturated acid solution with potentials lower than -0.1 V and showed relatively low band strength (Figure 8c). These

studies showed that *N_2H_x is generated on the Ru surface at a much faster rate than that of consumption/desorption. The spectral analysis suggested that the improvement of NRR performance needed to be reduced the binding strength of *N_2H_x species on the Ru surface. In another work, the NRR mechanisms on Rh surface were also employed via SEIRAS and differential electrochemical mass spectrometry (DEMS) by Yao et al.[34] They observed N_2H_x ($0 \leq x \leq 2$) with the stretching band of N≡N at ~2020 cm^{-1} via SEIRAS and the signal at $m/z = 29$ via DEMS. They proposed a new two-step reaction route on the surface of Rh, involving the formation of N_2H_2 via two-electron transfer processes, and then decomposed in the electrolyte to produce NH_3. According to the above analyses, the comprehensive NRR reaction mechanisms on the metal surface can be designed a balance between the dissolution of N_2 in the electrolyte and N_2 from the gas or electrolytes absorbed on metal surface. In this case, the NRR pathway on the metal surface may be carried out by the dissociation (dotted line) or association mechanism. The association pathways mainly include three processes: two-electron transfer, four-electron transfer and six-electron transfer. The exact association mechanism of NRR on certain metal surfaces can be decided by the rate determination step. For instance, when the energy barriers
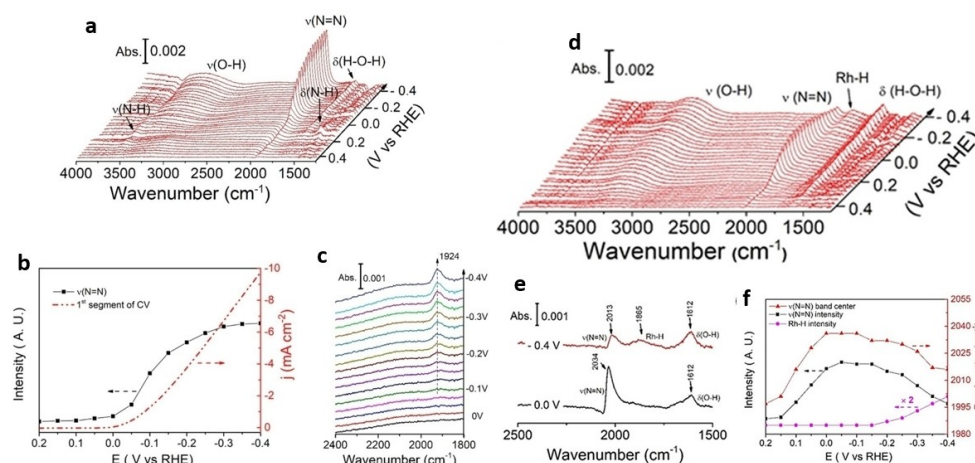
Figure 8. a) The infrared spectra on the Ru film electrode during the first segment from 0.4 to −0.4 V with N_2. b) The relations between the potential and the intensity of N≡N stretching band. c) The infrared spectra on the Ru film electrode for HER. d). The infrared spectra on Rh-film electrode with N_2; e) Single spectra at 0 V (black line) and −0.4 V (red line). f) The relations between potential and the strength of N≡N stretching band. Copyright 2019 American Chemical Society; Copyright 2020 Wiley-VCH.[33–34]

of N_2H_2 desorption are lower than those of further reduction of N_2H_2, the NRR will go through two electron transfer pathway and take N_2H_2 as the products, and then disintegrate into NH_3 and N_2 in the electrolyte. The process of four electron transfer pathway with N_2H_4 as by-products is similar to two electron transfer pathways. As for the dissociation pathway, only the six-electron transfer process involves ammonia as the only products. These findings will give the researches to further understand the NRR mechanisms on the metal surfaces via *in-situ* techniques, and also offer theoretical directions to develop the metal catalysts on NRR.

The mechanisms and the distributions of products as a function of applied voltages cannot be reproduced by a simple thermo-chemical model, when in the treatment of more complicated reactions, such as NRR. Thus, it required a more detailed model to investigate the NRR. Tayyebi et al. chose the electrochemical solid-liquid interface model to investigate the dynamics of NRR on Ru(0001).[35] They speculated that the hydrogenation of $N_{2,V}$ was converted to NNH_V, and then transferred to NNHH, which is one of the dominating path of NRR to NH_3 formation on Ru(0001) and that the optimal mechanism follows an associative distal pathway (Figure 9). Their reports may provide new viewpoint into the mechanism of metal-surface NRR reactions and further help to design more superior electro-catalysts.

From the volcano plots in Figure 4a, Pd has a high theoretical activity for HER, and it is not recommended to reduce nitrogen. Nevertheless, some experimental results have been reported that Pd metals could act as electro-catalysts for NH_3 synthesis. Wang et al. reported Pd nanoparticles dispersed on carbon black (Pd/C) as effective NRR catalysts with NH_3 yields of 4.5 $\mu g\,h^{-1}\,mg^{-1}_{Pd}$ and FEs of 8.2% in PBS solution (Figure 10a–b).[11] Controlled experiments indicated that PBS solution could effectively inhibit HER, and the NRR performance of Pd was much higher than those in acidic and basic media (Figure 10b). Meanwhile, DFT results indicated that α-PdH could

activate N_2 via thermodynamically more advantageous Grotthuss-like hydride transfer path, reducing the barrier potential of N_2 protonation to *N_2H, facilitating NRR process (Figure 10c). The surface modification of Pd nanoparticles can also enhance the catalytic activity. Sun et al. developed oxygen-rich tannic acid-modified Pd nanoparticles (Pd—TA) to boost the performance of electrochemical N_2 reduction to NH_3.[36] The as-grown Pd—TA catalysts achieved high NH_3 yields (24.12 $\mu g\,h^{-1}\,mg^{-1}_{Pd}$) and FEs (9.49%) with an applied voltage of −0.45 V vs RHE in the neutral media. Notably, the study also demonstrated long service time of the catalyst during the electrochemical reaction.

3.2. Metal alloy electrocatalysts for NRR

As an excellent catalyst, Ru is commonly used in the Haber-Bosch method in conventional ammonia synthesis. Theoretical studies have proved the catalytic mechanism (association and dissociation mechanism) on the surface of Ru. Considering the synergistic effect, combination with noble metals such as Pd and Pt, has the effect of maximizing catalytic performance.[37–40] The noble metal-based alloying electrocatalysts could weaken the H atoms binding and suppress the side reactions. For example, Manjunatha and Schechter developed RuPt/C catalysts for NRR with NH_3 yield of 6.37×10^{-10} mol $s^{-1}\,cm^{-2}$ and the homologous FE of 1.15% at −0.077 V vs RHE.[37] Additionally, higher FE was obtained at more positive voltages (Figure 10d). The performance of RuPt/C catalyst for electrochemical reduction of N_2 was attributed to a synergistic effect, the adsorption of N_2 molecules by Ru sites and the adsorption of H atoms by Pt sites for NH_3 synthesis. In another study, PdRu electrocatalysts with various nanostructures for NRR were developed. RuPd alloy with tripod structures was used as the efficient electro-catalysts with NH_3 yields of 37.23 $\mu g\,h^{-1}\,mg_{cat}^{-1}$ (1.94×10^{-10} mol $s^{-1}\,cm^{-2}$) and FEs of 1.85% (Figure 10e).[38] And it also exhibited good stabilities over 20 h. The nanorod PdRu alloy
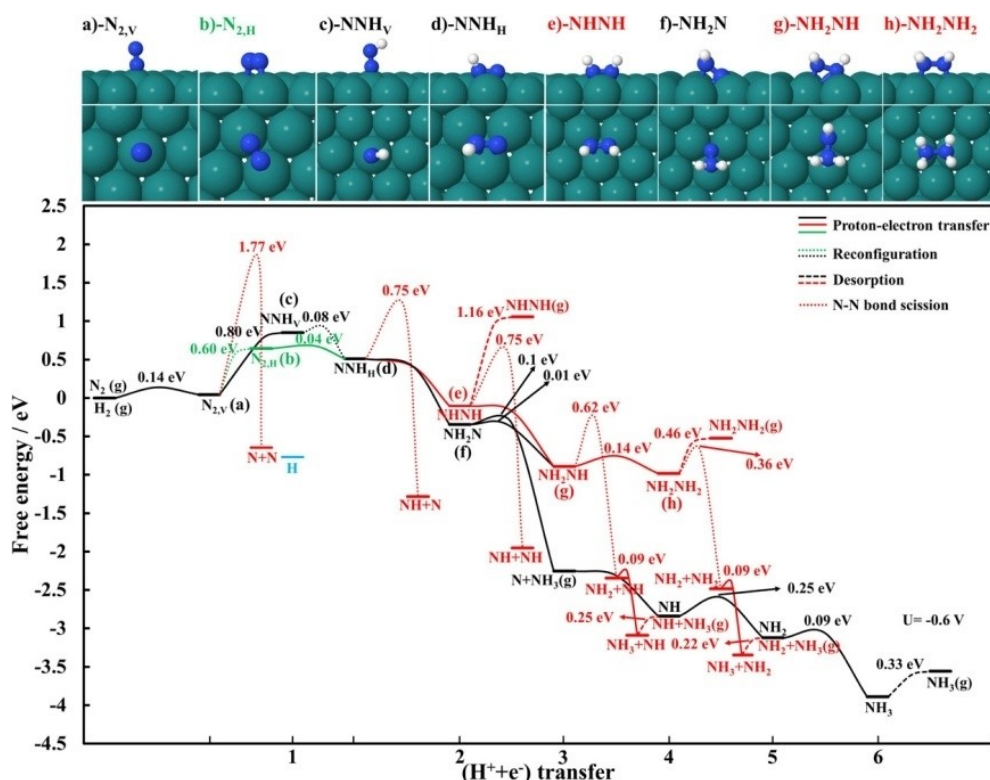
Figure 9. DFT calculations for NRR mechanism to ammonia formation on at a Ru(0001) electrode. Copyright 2019 American Chemical Society. [35]

was used as good electro-catalysts with NH_3 production rates of 34.2 $\mu g\,h^{-1}\,mg_{cat}^{-1}$ (5.62×10^{-11} $mol\,s^{-1}\,cm^{-2}$) and FEs of 2.4% (Figure 10f).[39] Even though the morphology of tripod showed a higher NH_3 production rate per milligram of catalyst, the morphology of nanorods is still a better structure based on the NH_3 yield per unit area. Wang et al. demonstrated that 3D bimetallic PdRu porous structures (3D PdRu BPNs) had enough active sites and beneficial electronic effects, which could be used as effective electrocatalysts for NRR. The NH_3 formation rates of 25.92 $\mu g\,h^{-1}\,mg_{cat}^{-1}$ could be achieved through a possible distal hydrogenation mechanism in acidic medium.[40]

Another consideration of electrocatalytic performance is loss of noble metals and the associated cost. The amount of precious metals can be lowered if they are combined with abundant transition metals (such as Cu, Fe, or Pb) on earth.[21a,41] Hence, transition-metal alloys have the capability of both high catalytic activity and low cost for electrochemical field.[42] For example, bimetallic catalysts of Pd_xCu_{1-x} dispersed on reduced graphene oxide (Pd_xCu_{1-x}/RGO, particle size of Pd_xCu_{1-x} was about 1.7 nm) were synthesized by reducing the precursors of Pd, Cu, and graphene oxide. (Figure 11a).[21a] The X-ray photo-electron spectroscopy results confirmed the alloy structures and the electronic interactions between the different ratios of Pd and Cu. The highest NH_3 yield rate of $Pd_{0.2}Cu_{0.8}$/RGO catalyst was 2.80 $\mu g\,mg_{cat}^{-1}\,h^{-1}$ and corresponding FE of 0.6% in an alkaline medium at applied voltage of -0.2 V vs RHE, and the highest FE was up to 4.6% at applied voltage of 0.0 V vs RHE, as given in Figure 11b. No hydrazine was detected, indicating that it had a good selectivity for the formation of NH_3. Additionally,

the NH_3 yields of $Pd_{0.2}Cu_{0.8}$/RGO catalyst displayed greatly larger than that of Pd/RGO, Cu/RGO, Pd, and Cu catalysts synthesized by the identical approach (Figure 11c) due to its nature of bimetals and amorphous structures. H was easily adsorbed on Pd atoms, which was probably covered by H_2, displaying low NRR catalytic activities. The introduction of Cu could accelerate the hydrogen desorption and improve the performance of NRR. Moreover, there were many dangling bonds in amorphous materials, which were the active sites of NRR. At present, there are few studies on amorphous precious catalysts for NRR. Researchers can pay more attention to the investigation of other amorphous precious metals accompanied by the defect engineering approaches or the control of morphology.

Moreover, Guo et al. demonstrated that 3D layered inter-connected porous structures of Pd_3Cu_1 catalysts of the NH_3 formation rates were as high as 39.9 $\mu g\,h^{-1}\,mg^{-1}$ at applied voltage of -0.25 V vs RHE.[41a] Chen et al. further studied the influence of Cu on NRR activity of RhCu bimetallic ultrathin nanoflake nanoaggregates (RhCu-BUNNs) via DFT calculations.[41b] The Cu introduction could effectively lower the energy barrier in the *NN reduction process of RhCu-BUNNs electrode with a smaller barrier of 0.16 eV, resulting in enhanced NRR (Figure 11d and 10e).[41b] The same phenomena were observed after the addition of Fe in bimetallic Ru—Fe nanoparticles supported on nanotubes (Ru_3Fe/CNTs) when used for NRR.[41c]

PdPb nanosponge was prepared for the first time and was applied as an electrocatalyst for NRR synthesis.[43] After introduction of plumbum (Pb) metal to the catalyst, the NH_3
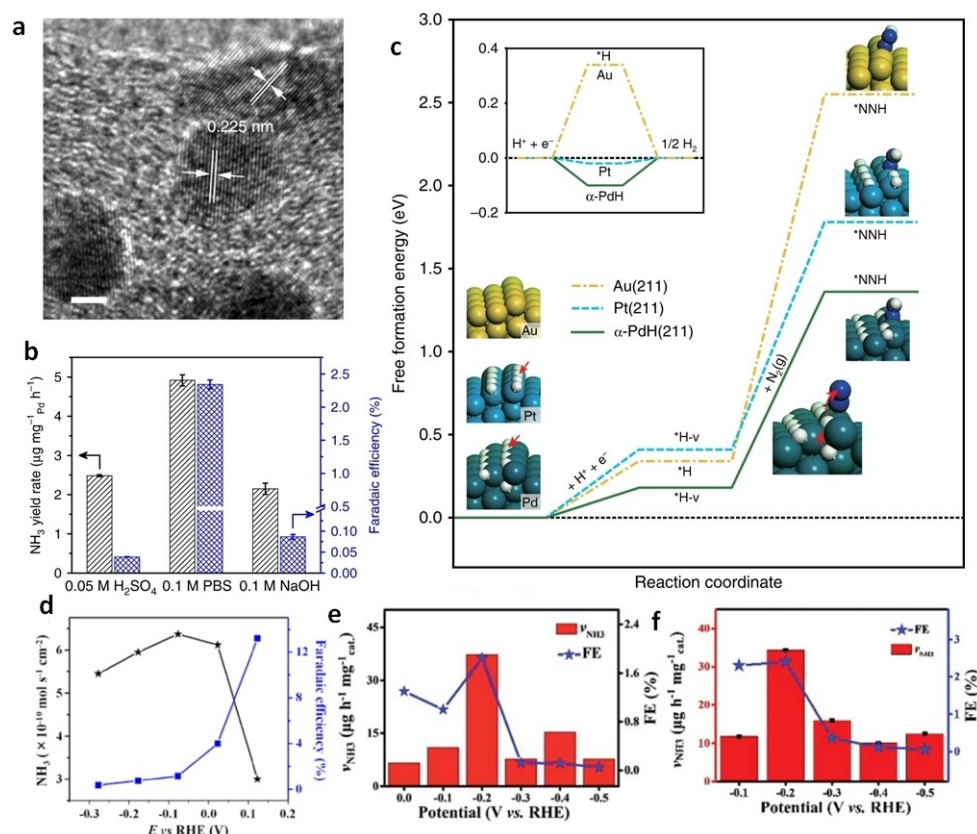
Figure 10. a) High-resolution electron transmission microscopy images of the Pd/C catalyst; b) NH₃ yield rates and FEs of Pd/C catalysts in different solutions; c) DFT calculations for the NRR mechanism. Copyright 2018 Springer Nature.[11] d) Correlation between NH₃ formation rates and FEs at various potentials. Copyright 2018 Elsevier B. V.;[37] e) NH₃ formation rates and FEs at selected voltages. Copyright 2019 The Royal Society of Chemistry;[38] f) The ammonium yield rates and homologous FE at the specific voltages. Copyright 2019 The Royal Society of Chemistry.[39]

formation rates were up to 25.68 $\mu g\,mg_{cat}^{-1}\,h^{-1}$ (5.14 $\mu g\,cm^{-2}\,h^{-1}$) at applied voltage of 0.05 V vs RHE in acidic solution. The corresponding FE was 5.79% and the catalytic effect was 8 times that of single-metal Pd/C (4.8 $\mu g\,mg_{cat}^{-1}\,h^{-1}$) (Figure 12a). DFT studies showed that Pb addition into PdPb could greatly inhibit the preferential adsorption of *H by catalysts and promote the adsorption of N₂, significantly reducing the energy barrier of forming *NNH in the rate-determining step of NRR, thus boosting the catalytic performance and selectivity of NRR (Figure 12b).

Other effective strategies, including defect engineering, crystal-phase engineering, and high-index facets, have been developed to modify the physical and chemical characters of catalysts to enhance their catalytic activities.[29b,44–46] For example, PdZn nanoparticles with rich defects loaded on N-doped hollow carbon (etched-PdZn/NHCP) were prepared by pyrolyzation of metal-organic framework (MOF) precursors, then went through an acid etching process.[44] The NH₃ yields of etched-PdZn/NHCP electro-catalysts were as high as 5.28 $\mu g\,mg_{cat}^{-1}\,h^{-1}$ and corresponding FEs of 16.9% in PBS solution. This kind of structures with abundant defects and porous carbon matrix could increase the usable charge density and facilitate mass transfer, which played a key role in accelerating acquisition and protonation of the N₂ molecules, thus realizing a desirable NRR capability and an effective HER suppression, as given in

Figure 12c–d. Huang et al. used a crystal-phase engineering strategy to prove that body-centered cubic (BCC) PdCu nanoparticles could be used as effective electro-catalysts for NH₃ production (Figure 13a and b).[45] BCC PdCu achieved high NH₃ yields of 35.7 $\mu g\,mg_{cat}^{-1}\,h^{-1}$, high FE of 11.5%, and good selectivity (no detected N₂H₄) at an applied voltage of −0.1 V vs RHE, which was a higher performance than that of face-centered cubic PdCu. ¹⁵N-tracer method was carried out to confirm the source of the NH₃ formation (Figure 13c). DFT calculation revealed that, profiting by structure engineering, the surface Cu 3d band acted as a valid d-d coupling relevant center to overcome the energy barrier and boosted the Pd-4d electron exchange and transfer activities towards superior reduction N₂ to NH₃ (Figure 13d). In another study, excavated cubic Pt₉₃Ir₇ alloy nanocrystals with high-index {710} facets showed superior electro-catalytic activity for NRR with a FE of 40.8% and NH₃ yield of 28 $\mu g\,h^{-1}\,cm^{-2}$.[29b] DFT results demonstrated that Ir atoms decorated Pt stepped surface could inhibit HER and greatly promote N₂ reduction to NH₃ (Figure 13e and f). Surface plasma treatments are also widely applied in the electrochemical field.[46a] Xiong et al. used in-situ synchrotron radiation-based infrared spectroscopy and X-ray photoelectron spectroscopy to prove that surface plasmons of Au–Ru nano-structures could provide enough energy to activate N₂ via a
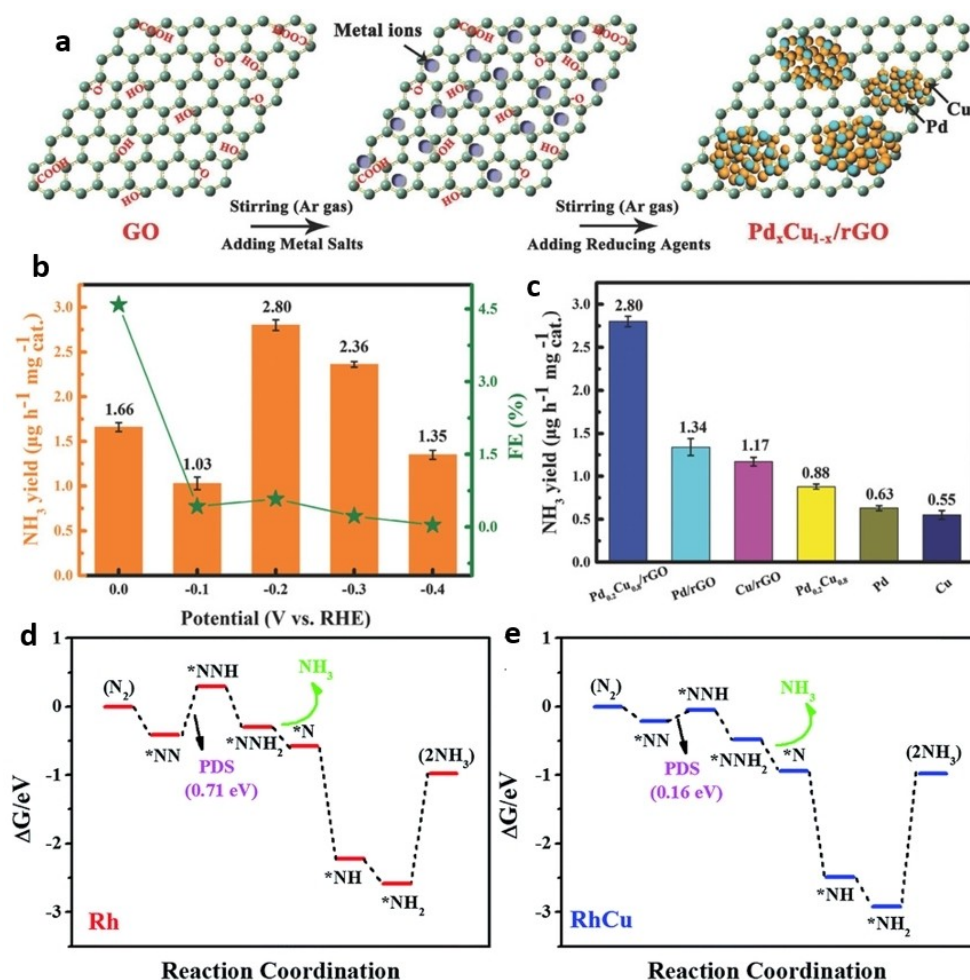
Figure 11. a) Schematic diagram of the grown of Pd$_x$Cu$_{1−x}$/rGO; b and c) Electrocatalytic NRR of Pd$_x$Cu$_{1−x}$/rGO composites. Copyright 2018 Wiley-VCH.[21a] The energy barrier curves for NRR on the Rh-BUNN (d) and RhCu-BUNN (e) electrodes. Copyright 2019 The Royal Society of Chemistry.[41b]

dissociation mechanism in the existence of water and incident illumination.[46a]

The synergistic effect of two-component alloy can improve electro-catalytic activities, so it is worth investigating whether three-component alloys can go deep into the improvement of the activities. Considerable reports have been discussed this problem from both theoretical and experimental aspects. For instance, long-spine urchin-like structure of PdCuIr (PdCuIr-LS) was prepared by a facile one-pot method.[47] PdCuIr-LS exhibited excellent catalytic performance for NRR with NH$_3$ formation rates of 13.43 µg mg$_{cat}^{-1}$ h^{-1} and FEs of 5.29% in the neutral medium, due to its hyper-branched structure and tri-metallic composition effect.

As evidenced from the results, the strategies of alloys can enhance the noble metal-based electro-catalysts of NH$_3$ conversion efficiency because the binding of H-adatoms was weaken, restraining the competitive HER. Meanwhile, the same catalysts display the different catalytic activities for NRR, which is affected by many factors including structures, morphologies, compositions, and defects. For instance, the catalysts with more exposed edges and large specific surface area will exhibit better NRR performances in the case of the same other conditions.

However, it is noteworthy that the alloying effect may not break the scaling of *N$_2$H and *NH$_2$, owing to their formation of the similar bonds on the surface by a single N atom. Hence, the design of the active sites of the alloys is obliged to alter the binding configuration of these intermediates and also take into account of the factors of the morphologies, compositions and defects in the follow-up studies.

3.3. Heterojunction structure electro-catalysts for NRR

Fundamental structural studies show that metal oxide interfaces play a significant role in enhancing catalytic performance for electrochemical field owing to strong interface interaction,[48] especially the interfacial constraint effect between metal and metal oxide.[49] As a result, there is urgent need for further design of heterojunctions to accelerate the NRR dynamic process. Recently, Liang et al. published two articles on Pd-based heterogeneous catalysts, which could be used as an electro-catalyst with a balance of the HER and NRR reaction, and meanwhile improved the selectivity of NRR and the yield of NH$_3$.[46c,49] PdO/Pd hybrids loaded on carbon nanotubes (PdO/
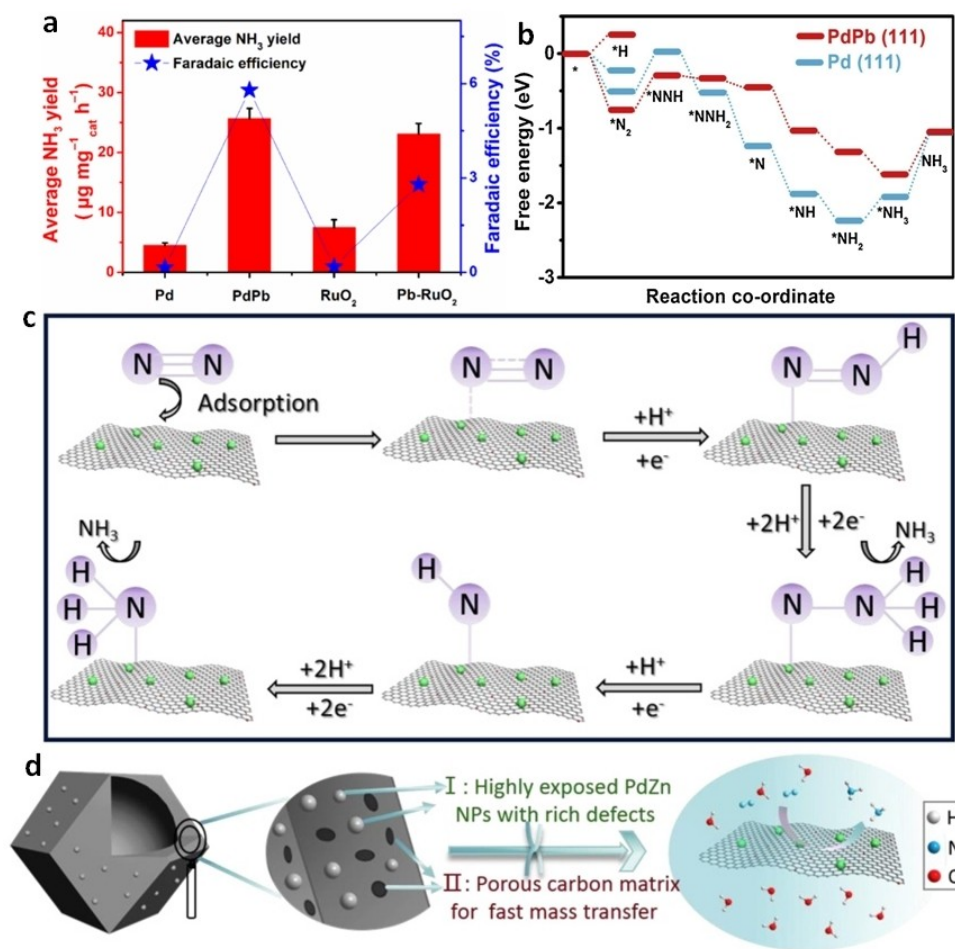
Figure 12. a) NH₃ yields and FEs of various catalysts at 0.05V vs. RHE in acidic media; b) The energy barrier illustration for NRR of NRR of PdPb (111) and Pd (111). Copyright 2020 Elsevier B. V.;[43] c) The reaction pathway of NRR on the etched-PdZn/NHCP electrode. d) Schematic diagram of the etched-PdZn/NHCP electrodes for NRR. Copyright 2018 Elsevier B. V..[44]
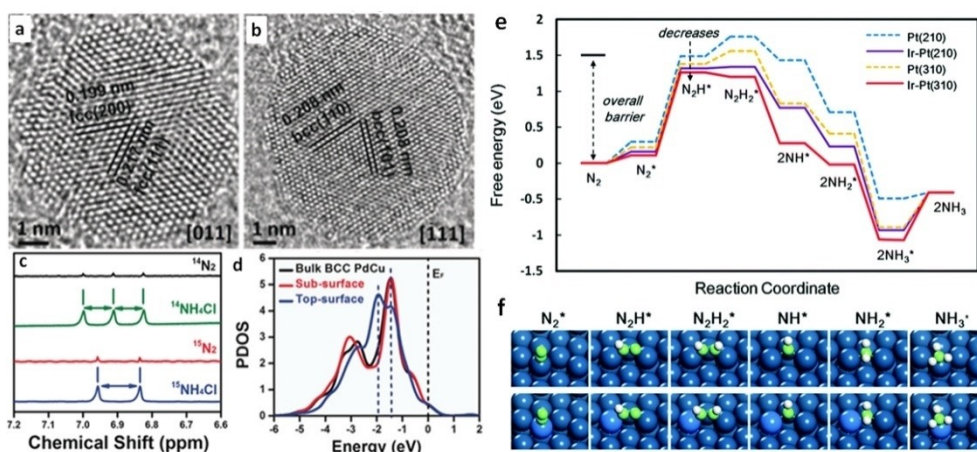

Figure 13. HRTEM image of PdCu/C (a) and PdCu/C-350 (b); c) ¹H NMR plots of the electrolyte with ¹⁵N₂ and ¹⁴N₂ of PdCu/C-350 for NRR; d) The partial density of states (PDOSs) of the Cu-3d band in BCC PdCu. Copyright 2020 Wiley-VCH.[45] DFT analysis (e) and optimal structure of intermediates (f) for NRR on Pt and Ir modified Pt surfaces. Blue: Pt; cyan: Ir; green: N; white: H. Copyright 2019 The Royal Society of Chemistry.[29b]

Pd/CNTs) by adjusting the mass ratio of Pd/PdO were fabricated. The catalytic activities of PdO/Pd/CNTs was greatly boosted for NRR with FEs of 11.5% and the NH₃ formation rate

of 18.2 µg mg$_{cat}^{-1}$ h^{-1} at an applied voltage of 0.1 V vs RHE. The authors further investigated the relevance between the irradiation time and reduction degree, and revealed that an

appropriate reduction degree was advantageous to NRR (Figure 14a). The interfaces between the PdO and Pd could boost the catalytic activities of NRR, in which the Pd adsorption of N_2 to form chemisorption bonds of Pd–N_2, while the PdO transmission of protons to form α-PdH and cleaved the N≡N triple bond (Figure 14b). The synergism of Pd and PdO effectively reduced the protons transition distance and the energy barrier of the chemical reaction.

Another example of heterogeneous catalysts was Ru/2H–MoS$_2$, which showed excellent catalytic activity for NRR with FEs of 17.6% and NH_3 production rate of 1.14×10^{-10} mol cm^{-2} s^{-1} at 50 °C.[50] Both experimental and theoretical evidences showed that the interfaces between Ru and 2H–MoS$_2$ could boost the catalytic activities of NRR, in which the Ru offered the sites for activating N_2 binding and the S-vacancy of the 2H–MoS$_2$ provides the sites for activating H$^+$ binding (Figure 14c–e). Therefore, the method to adopt semiconducting materials could go deep into expansion of catalytic materials for other reactions restricted by the side effect, such as the reduction of carbon dioxide.

Recently, the design of heterojunction structures is considered as one of the effective methods to boost the NRR catalytic activities. However, the direct evidence on how these components function is still lacking. For example, "synergy effect" has not been deeply analyzed, and the relationships between phase, interface, material and defect are not fully understood. In the next researches, the intermediates of NRR will be observed by the in-situ measurements, which will help us to explore and confirm the synergy effect, so that a single catalyst can preferably integrate the merits of multicomponent materials.

3.4. Noble metal compounds for NRR

As described above, α-PdH formation during electrochemical process can improve the catalytic performance through a hydride migration mechanism. Based on this premise, nanoporous palladium hydride were prepared by a dealloying method and used as an excellent electro-catalyst for NRR with the NH_3 formation rates of 20.4 mg h^{-1} mg$_{cat}^{-1}$ and FEs of
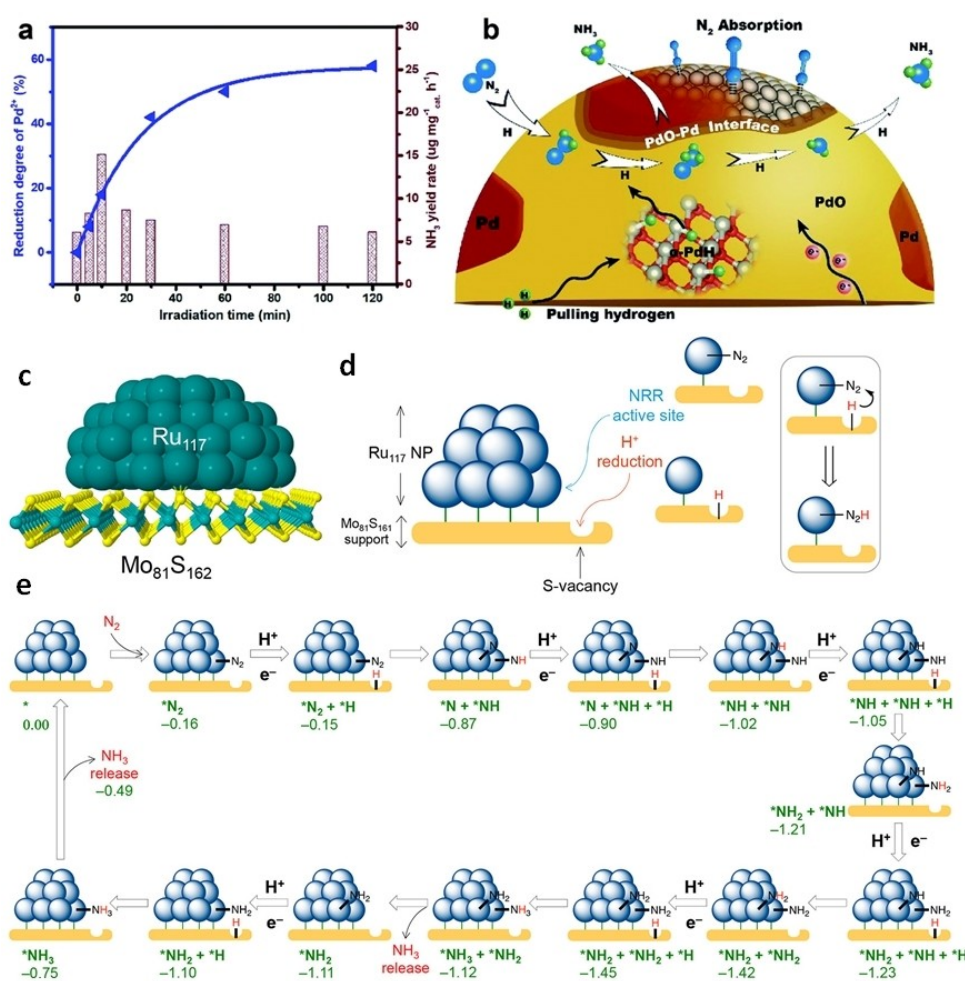

Figure 14. a) The relations between reductive degree (blue) and NH_3 formation rates (brown) of the catalysts; b) NRR mechanism on the PdO-Pd interface at normal temperature and pressure. Copyright 2019 The Royal Society of Chemistry;[49] DFT calculations for the NRR mechanism on the Ru/2H–MoS$_2$ electrode (c–e). Copyright 2018 American Chemical Society.[50]

43.6%.[21b] They also used isotopic tracer methods to understand the mechanism of NRR on nanoporous-PdH$_{0.43}$. Isotopic ^{15}N labeling experiment was carried out to confirm the NH$_3$ product from the source of N (Figure 15 **a**). *In-situ* Raman spectra and DFT calculations demonstrated that N$_2$ was activated and effectively converted into *N$_2$H (Figure 15b–e).

Other strategies have also been applied to noble metal compounds. Doping catalyst materials with heteroatoms (such as N,[51] P,[51c,52] S[53]) can effectively tune their intrinsic properties and are widely used in the electrochemical. It is well known that P with negative charge can cause the deviation of electron cloud density in the metals, thus regulating the surface charge state of transition metals, promoting the intermediate of catalytic process and boosting the intrinsic catalytic performance. Recently, RhP$_x$ nanoparticles implanted in N, P dual-doped carbon film (RhP$_x$@NPC) were synthesized by means of sacrificial template and pyrogenic decomposition.[51c] Rh$_2$P@NPC displayed superior electro-catalytic performance for NRR. The NH$_3$ formation rates and FEs were up to as high as 37.6 µg h^{-1} mg$_{cat}$$^{-1}$ at the applied voltage of −0.25 V and 7.64% at −0.05 V in the acidic medium, respectively. The authors used ^{15}N isotopic tracer to confirm the NH$_3$ product from the actual N source. In addition, DFT analysis demonstrated that the doping of P into RhP$_x$@NPC could regulate the electronic structure of Rh, allowing the N≡N bond to easily combine with Rh, thus promoting the catalytic performance (Figure 15f–l). In the same way, the introduction of Pd and P elements into Au nanowires could also efficiently adjust their electronic structures and acted as superior electro-catalysts for NRR.[52]

Glassy materials, also known as amorphous materials, also provide a broad application prospect in the field of NRR, owing to their special properties of disordered atomic arrangement and excellent abilities of anti-corrosion.[54] These materials can offer more defect sites than their crystalline counterparts, which are used as trapping sites for metastable electrons and noble gas molecules.

For example, a category of vitreous bullet-like M–Te (M≡Ru, Rh, Ir) porous nanorods (PNRs) were prepared by simple hydrothermal approaches.[54] The IrTe$_4$ PNRs exhibited excellent NRR activities with high FEs of 15.3% and NH$_3$ production rate of 51.1 µg h^{-1} mg$_{cat}$$^{-1}$, outperforming many reported NRR electro-catalysts. The reaction mechanisms of IrTe$_4$ PNRs for NRR in alkaline media were calculated by DFT, based on the electronic structure and energy path of IrTe$_4$ PNRs. Ir was considered to dissociate H$_2$O and inject electrons into Te to stabilize N$_2$. Meanwhile, IrTe$_4$ PNRs displayed a much higher potential barrier for HER in basic solutions, which was 0.33 eV. The whole endothermic HER processes in IrTe$_4$ PNRs enhanced the activities of NRR, according to the evidence of the inhibition of HER (Figure 16). This study offers new insight into the development of high-efficiency electrocatalysts with glassy structure for NRR. Similarly, another work using Ru–Pt$_{18}$Te$_{17}$ sheets also demonstrated a boost to catalytic activity for NRR via the control of proton or electron velocity.[55] This finding opens up a new perspective for the experimental and theoretical direction to novel NRR catalysts.

Generally, it is easy for the heterogeneous to separate from reactant/product/electrolyte mixtures. Therefore, high cost of noble metal-based catalysts is effectively recycled, which make them appealing for potential practical application. Noble metal (Group VIII)-based heterogeneous catalysts have been investigated for electro-catalytic NRR in this review, and we also give a brief summary of the NRR performances using various heterogeneous catalysts, listed in Table 4. It can be obviously found that the performance of noble metal heterogeneous catalysts is superior to other heterogeneous catalysts due to their good conductivity and the abilities with easy adsorption of reactants and stable reaction intermediates. However, there are still some issues for heterogeneous catalysts to be addressed. For instance, the heterogeneous catalysts and electrolytes are in the solid and liquid phases, respectively. The whole NRR activities of the heterogeneous electro-catalysts are subject to the mass transfer from the liquid phase to the solid
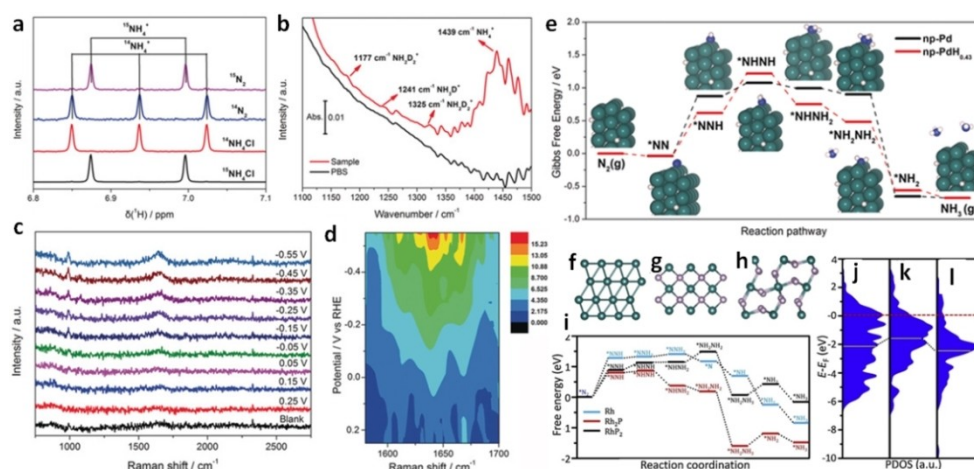

Figure 15. a) Baseline-subtracted ^{1}H NMR spectra. b) The infrared spectra in the solution with isotope substituted catalyst. c) *In-situ* Raman spectra and d) relevant contour plots of np-PdH$_{0.43}$ at different voltages. Copyright 2020 Wiley-VCH.[21b] f) Rh (111), g) Rh$_2$P (200) and h) RhP$_2$ (−111) of side view structures. i) DFT calculations for NRR pathways on different electrodes; j–l) PDOSs for the Rh -*d* band on the surface of different catalysts. Copyright 2020 Elsevier B. V..[51c]
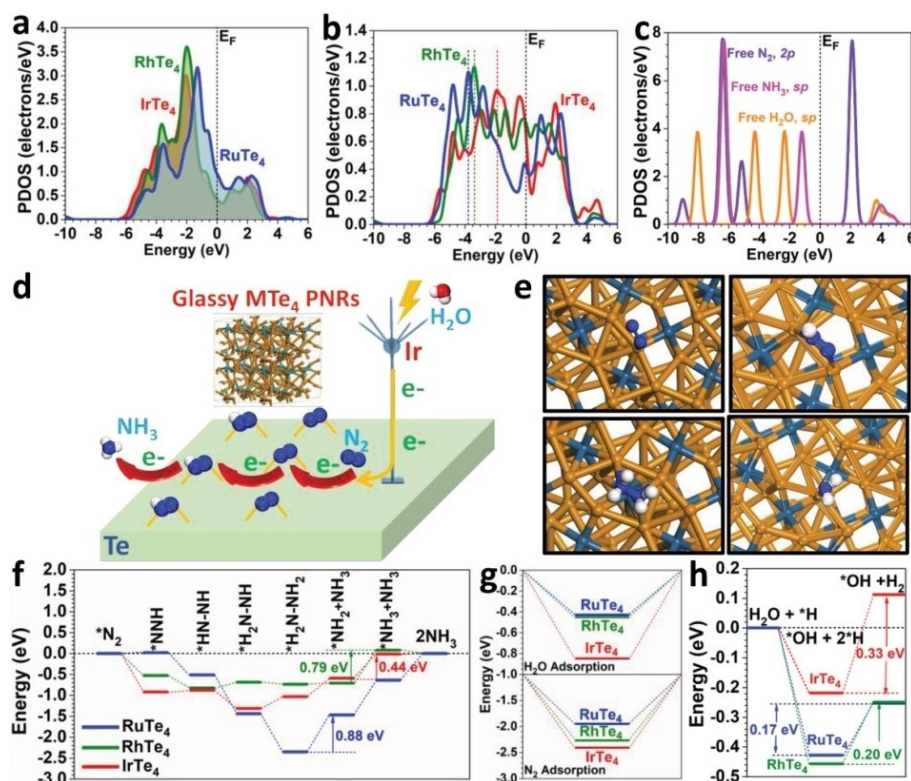
Figure 16. The PDOSs of metal-d band (a), 4p band of Te (b), and main intermediate in NRR (c); The electrons transfer of M—Te PNRs (d); Optimal structure of main intermediate for NRR (e); NRR reaction pathway of M—Te PNRs (f); The comparisons between N_2 and H_2O on the adsorption energy (g); HER reaction path of the M—Te PNRs (h).[54] Copyright 2020 Wiley-VCH.

Table 4. A brief summary of the NRR performance using various heterogeneous catalysts.

Catalyst	NH_3 yield	FE%	Electrolyte	Potential (V vs RHE)	Ref.
Ru SAs/N–C	120.9 $\mu g_{NH3} mg_{cat} h^{-1}$	29.6%	0.05 M H_2SO_4	−0.2	Adv. Mater., 2018, 30, 1803498
Ru SAs/g–C_3N_4	23 $\mu g_{NH3} mg_{cat} h^{-1}$	8.3%	0.5 M NaOH	0.05	Adv. Funct. Mater., 2020, 30, 1905665
Pd/C	4.5 $\mu g_{NH3} mg_{cat} h^{-1}$	8.2%	0.1 M PBS	0.1	Nat. Commun., 2018, 9, 1795
RhCu-BUNNs	95.06 $\mu g mg^{-1}_{cat} h^{-1}$	2%	0.1 M KOH	−0.2	J. Mater. Chem. A 2019, 7, 21149–21156
BCC PdCu	35.7 $\mu g mg^{-1}_{cat} h^{-1}$	11.5%	0.5 M LiCl	−0.1	Angew. Chem. Int. Ed., 2020, 59, 2649
$Pt_{93}Ir_7$ alloy	28 $\mu g h^{-1} cm^{-2}$	40.8%	1 mM HCl	−0.3	Chem. Commun., 2019, 55, 9335–9338
PdO/Pd/CNTs	18.2 $\mu g_{NH3} mg_{cat} h^{-1}$	11.5%	0.1 M KOH	−0.1	J. Mater. Chem. A, 2019,7, 12627–12634
Fe_2O_3–CNT	0.22 $\mu g h^{-1} cm^{-2}$	0.15%	2 M NaHCO₃	/	Angew. Chem. Int. Ed., 2017, 56, 2699
Fe plate	$2.8 \times 10^{-3} \mu g h^{-1} cm^{-2}$	1.0%	6 M KOH	/	J. Electrochem. Soc. 1983, 130, 734–735
TiO_2 NS array	5.61 $\mu g h^{-1} cm^{-2}$	2.5%	0.1 M Na_2SO_4	−0.7	ACS Appl. Mater. Interfaces, 2018, 10, 28251–2825
VN NS array	5.14 $\mu g h^{-1} cm^{-2}$	2.25%	0.1 M HCl	−0.5	ACS Sustainiable Chem. Eng., 2018, 6, 9545–9549
Fe_3O_4 nanorod	3.43 $\mu g h^{-1} cm^{-2}$	2.6%	0.1 M Na_2SO_4	−0.4	Nanoscale, 2018, 10, 14386–14389
MoS_2	4.94 $\mu g h^{-1} cm^{-2}$	1.17%	0.1 M Na_2SO_4	−0.5	Adv. Mater., 2018, 30, e1800191
NPC	0.97 $\mu g mg^{-1}_{cat} h^{-1}$	4.2	0.1 M HCl	−0.8	Chem. Commun., 2019, 55, 687–690

Note: NS refers to nanosheet; NPC refers to N/P co-doped hierarchical porous carbon.

phase. Moreover, the surface chemical properties of the active sites on heterogeneous catalysts are often inhomogeneous, which makes it more complicated to understand their reaction mechanisms and obtain high reaction selectivity. If the single strategy is not to obtain high FEs for the NRR, we will develop the associated approaches to the design of the electro-catalysts, which will satisfy the requirements for optimized N_2 adsorption and successful inhibition of HER. These potential strategies also require the continuous development of theoretical understanding of NRR reaction mechanisms. Hence, the researchers need

to consider the aforementioned factors when designing electro-catalysts for NRR.

4. Conclusions and Outlooks

Electro-catalytic NRR is considered to be an eco-friendly alternative to the conventional Haber-Bosch method, and a potential prospect to foster renewable energy sources via the chemical bonds. Recently, great progress in improving the NH_3

yield rates and efficiencies have been made. In the review, we provide the fundamental thermodynamics and mechanisms of NRR and the detection ammonia methods. Rational strategies for constructing efficient electrochemical system of noble metal (VIII)-based electro-catalysts for NRR have been provided and the performances of them are summarized in Table 5. Despite the great progress has been made in recent years, the design and development of efficient electro-catalysts for NRR are still a main challenge, which include low NH_3 formation rates, high applied voltages, the poor NRR selectivity, because the redox potential of the HER is similar to that of NRR, but its reaction kinetic is faster than that of NRR, which requires a lot of in-depth researches in this field. Thus, it is very desirable development of high efficiency of electro-catalysts with high NH_3 yield rates and good NRR conversion. Electro-catalytic NRR is one of the possible ways to realize the synthesis of NH_3; however, there are still several main problems to be addressed:

(1) Suppressing HER: The almost all present NRR electro-catalysts toward NH_3 formation in aqueous systems display extremely low catalytic activity and selectivity. This is mainly caused by the domination of HER as the electron and proton transmit to produce H_2. In addition, the specific catalytic performance of precious metals to NRR still needs to be strengthened and the loading amount of them should be markedly reduced. Hence, in order to largely enhance the catalytic activities and selectivity of NRR, it is necessary to adopt strategies to inhibit or even circumvent HER. Morphology engineering, defects engineering, crystal facet engineering, heteroatom doping, and synergistic interface engineering are considered as good options to restrain HER and improve NRR. For example, encapsulation of electro-catalysts with zeolite imidazole framework could reduce the H atom absorption on the catalyst surface, which is a helpful way to inhibit HER.[56] Another practical method is to inhibit HER by increasing N_2 solubility.[6] In addition, high concentration of K^+ as the support electrolytes, could be used to slow down the migration of protons, leading to the suppression of HER.[57] Meanwhile, the inhibition degree of HER would be enhanced with the increase of K^+ concentration.

Table 5. Summaries of various noble metal-based electro-catalysts for NRR.

Catalyst	NH_3 yield	FE%	Electrolyte	Potential (V vs RHE)	Ref.
Ru cathodes	$1.30 \mu g\, h^{-1} cm^{-2}$	0.24%	2 M KOH	−1.02	Chem. Commun., 2000, 1673–1674.
Ru SAs/N–C	$120.9\ \mu g_{NH3}\, mg_{cat} h^{-1}$	29.6%	0.05 M H_2SO_4	−0.2	Adv. Mater., 2018, 30, 1803498
Ru SAs/g–C_3N_4	$23\ \mu g_{NH3}\, mg_{cat} h^{-1}$	8.3%	0.5 M NaOH	0.05	Adv. Funct. Mater., 2020, 30, 1905665
Ru dispersed ZIF-8	$16.68\ \mu g\, mg^{-1}_{cat} h^{-1}$ at −0.4 V	14.23% at −0.3 V	0.1 M KOH		Catal. Sci. Technol., 2020, 10, 1336–1342
Rh nanosheets	$23.88\ \mu g_{NH3}\, mg_{cat} h^{-1}$	0.217%	0.1 M KOH	−0.2	J. Mater. Chem. A, 2018, 6, 3211–3217
3D Rh particles	$35.58\ \mu g_{NH3}\, mg_{cat} h^{-1}$	0.52%	0.1 M KOH	−0.2	Chem. Asian J., 2020, 15, 1081–1087
Pd/C	$4.5\ \mu g_{NH3}\, mg_{cat} h^{-1}$	8.2%	0.1 M PBS	0.1	Nat. Commun., 2018, 9, 1795
Pd NPs	$24.12\ \mu g_{NH3}\, mg_{cat} h^{-1}$	9.49%	0.1 M Na_2SO_4	−0.45	J. Mater. Chem. A, 2019,7, 21674–21677
RuPt/C	$6.37*10^{-10}\ mol\, s^{-1} cm^{-2}$	1.15%	1 M KOH	−0.077	*Electrochem. Commun.*,2018, 90, 96–100
PdRu tripods	$37.23\ \mu g\, mg^{-1}_{cat} h^{-1}$	1.85%	0.1 M KOH	−0.2	J. Mater. Chem. A, 2019, 7, 801–805
PdRu nanorod	$34.2\ \mu g\, mg^{-1}_{cat} h^{-1}$	2.4%	0.1 M HCl	−0.2	Nanoscale, 2019, 11, 5499–5505
3D PdRu BPNs	$25.92\ \mu g\, mg^{-1}_{cat} h^{-1}$	1.53%	0.1 M HCl	−0.1	ACS Sustainable Chem. Eng., 2019, 7, 2400–2405
mAu_3Pd/Ni foam (NF)	$24.02\ \mu g\, mg^{-1}_{cat} h^{-1}$	18.16%	0.1 M Na_2SO_4	−0.1	ACS Appl. Mater. Interfaces, 2020, 12, 436–442
$Pd_{0.2}Cu_{0.8}$/rGO	$2.80\ \mu g\, mg^{-1}_{cat} h^{-1}$	3%	0.1 M KOH	−0.2	Adv. Energy Mater. 2018, 8, 1800124
Pd_3Cu_1	$39.9\ \mu g\, mg^{-1}_{cat} h^{-1}$	1.22%	1 M KOH	−0.25	Nano Energy, 2019, 58, 834–841
RhCu-BUNNs	$95.06\ \mu g\, mg^{-1}_{cat} h^{-1}$	2%	0.1 M KOH	−0.2	J. Mater. Chem. A,2019, 7, 21149–21156
PdPb/C	$37.68\ \mu g\, mg^{-1}_{cat} h^{-1}$ ($7.54\ \mu g\, cm^{-2} h^{-1}$)	1.19%	0.1 M HCl	−0.05	Appl. Catal. B-Environ., 2020, 265, 118481
Ru_3Fe/CNTs	$16.2\ mol_{NH3}\ h^{-1} g_{Ru}^{-1}$	/	/	/	Chem. Eng. Technol., 2020, 43, 719–730
PdZn/NHCP	$5.28\ \mu g\, mg^{-1}_{cat} h^{-1}$	16.9%	0.10 M PBS	−0.2	Appl. Catal. B-Environ., 2020, 265, 118568
BCC PdCu	$35.7\ \mu g\, mg^{-1}_{cat} h^{-1}$	11.5%	0.5 M LiCl	−0.1	Angew. Chem. Int. Ed.,2020, 59, 2649 −2653
$Pt_{93}Ir_7$ alloy	$28\ \ \mu g\, h^{-1} cm^{-2}$	40.8%	1 mM HCl	−0.3	Chem. Commun., 2019, 55, 9335–9338
AuRu	$101.4\ \mu mol\, g^{-1} h^{-1}$	0.21%	pure wate	/	J. Am. Chem. Soc.2019, 141, 7807–7814
PdCuIr–LS	$13.43\ \mu g\, mg^{-1}_{cat} h^{-1}$	5.29%	0.1 M Na_2SO_4.	−0.3	J. Mater. Chem. A, 2019, **7**, 3190–3196
PdO/Pd/CNTs	$18.2\ \mu g_{NH3}\, mg_{cat} h^{-1}$	11.5%	0.1 M KOH	−0.1	J. Mater. Chem. A, 2019,7, 12627–12634
Pd/TiO_2	$1847.3\ \mu g\, mg^{-1}_{cat} h^{-1}$	2.63%	0.1 M NaOH	−0.1	J. Colloid. Interf. Sci.,2019,553, 126–135
Ru/2H–MoS_2	$1.14*10^{-10}\ mol\, cm^{-2} s^{-1}$	17.6%	10 mM HCl	−0.15	ACS Energy Lett., 2019, 4, 430–435
np-PdH0.43	$20.4\ \mu g\, mg^{-1}_{cat} h^{-1}$	43.%	0.10 M PBS	−0.15	Angew. Chem. Int. Ed., 2020, 59, 3511–3516
Rh_2P@NPC	$37.6\ \mu g\, mg^{-1}_{cat} h^{-1}$ at −0.25 V	7.64% −0.05 V	0.05 M H_2SO_4		Appl. Catal. B-Environ., 2020, 256, 118589
AuPdP NWs	$18.78\ \mu g\, mg^{-1}_{cat} h^{-1}$ ($7.51\ \mu g\, h^{-1} cm^{-2}$)	15.44%	0.1 M Na_2SO_4	−0.3	ACS Sustainable Chem. Eng. 2019, 7, 15772–15777
Rh–Se NCs	$175.6 \pm 23.6\ mg\, h^{-1} g^{-1}_{Rh}$	13.3	0.1 M HCl	−0.1	Adv. Mater., 2020, 32, 2001267
$IrTe_4$ PNRs	$51.1\ \mu g\, mg^{-1}_{cat} h^{-1}$	15.3%	0.1 M KOH	−0.2	Adv. Mater., 2020, 32, 1907112

(2) Design of electro-catalyst structures: The nitrogen adsorption and activation happen on the active sites of the catalysts. Controlling the size of the catalysts can improve the availability of the catalysts, exposing more active sites to adsorb and activate N_2. Additionally, some special structures (such as nanorods, tripods, 3D structures) also boost the NRR activity. Thus, the morphology engineering may be an effective method to promote the NH_3 synthesis. As mentioned above, the catalyst performance is affected by the electron transport. The alloying and heteroatom doping methods can adjust the electronic structure of catalysts. It should be noted that the activity of the catalysts largely depends on the alloy ratio and the heteroatom content. Thus, it is needed to optimize the alloy ratio and the doping concentration.

(3) Combing theoretical calculations and advanced experimental techniques to design efficient catalysts: According to theoretical calculations and advanced experimental techniques, the competition between NRR and HER can be studied at the atomic levels. Nevertheless, it should be noted that a great deal of theoretical studies are mainly based on proper simplified models, which cannot exactly clarify the electro-catalytic process of NRR and may bring about some discrepancies between the experimental and theoretical results. Thus, in-depth research is needed to synergistically combine theoretical studies with advanced experimental techniques with *in-situ* characterization skills, such as *in-situ/operando* X-ray photoelectron spectroscopy (XPS), *in-situ* TEM, and *in-situ* synchrotron radiation technology. Feedbacks from these studies will be of great value to guide the development and manufacture of electro-catalysts with excellent activities for NRR.

(4) Exploitation of NRR electrochemical measurements: So far, the Tafel analysis for NRR has been limited. Further studies of NRR using rotating disk electrodes (RDE) or rotating ring disk electrodes (RRDE) are recommendable to explore the dynamics of the electrodes and the behaviors of electron transport at the given voltage, which are often applied in other electro-catalytic processes, such as oxygen reduction reaction (ORR), OER, and HER.

In conclusion, the tremendous advances of NRR have confirmed the possibilities of electro-reduction N_2 for NH_3 production using noble metal catalysts at normal temperatures and pressures. Although the present situation is less desirable according to the considerations from economic and practical aspects, we believe that, according to experimental and theoretical studies combining with *in-situ/operando* characterization techniques and exact measurements for determining the ammonia, will further promote to design and develop heterogeneous electro-catalysts of NRR with excellent catalytic active activities, high efficiencies, superior selectivity and stability in the near future.

Conflict of Interest

The authors declare no conflict of interest.

[1] a) C. Tang, S. Z. Qiao, *Chem. Soc. Rev.* **2019**, *48*, 3166–3180; b) C. Guo, J. Ran, A. Vasileff, S.-Z. Qiao, *Energy Environ. Sci.* **2018**, *11*, 45–56; c) G. F. Chen, S. Ren, L. Zhang, H. Cheng, Y. Luo, K. Zhu, L. X. Ding, H. Wang, *Small Methods* **2018**, *3*, 1800337.

[2] a) Y. Luo, G.-F. Chen, L. Ding, X. Chen, L.-X. Ding, H. Wang, *Joule* **2019**, *3*, 279–289; b) G. Zheng, J. M. Yan, G. Yu, *Small Methods* **2019**, *3*, 1900070; c) H. Huang, F. Li, Q. Xue, Y. Zhang, S. Yin, Y. Chen, *Small* **2019**, *15*, 1903500.

[3] H. Liu, L. Wei, F. Liu, Z. Pei, J. Shi, Z.-j. Wang, D. He, Y. Chen, *ACS Catal.* **2019**, *9*, 5245–5267.

[4] a) V. Kyriakou, I. Garagounis, E. Vasileiou, A. Vourros, M. Stoukides, *Catal. Today* **2017**, *286*, 2–13; b) Y. Yao, J. Wang, U. B. Shahid, M. Gu, H. Wang, H. Li, M. Shao, *Electrochem. Energy Rev.* **2020**, *3*, 239–270; c) H. Yu, Z. Wang, S. Yin, C. Li, Y. Xu, X. Li, L. Wang, H. Wang, *ACS Appl. Mater. Interfaces* **2019**, *12*, 436–442; d) H. Cheng, L. X. Ding, G. F. Chen, L. Zhang, J. Xue, H. Wang, *Adv. Mater.* **2018**, *30*, e1803694.

[5] a) D. Yan, H. Li, C. Chen, Y. Zou, S. Wang, *Small Methods* **2018**, *3*, 1800331; b) H. Tanaka, H. Mori, H. Seino, M. Hidai, Y. Mizobe, K. Yoshizawa, *J. Am. Chem. Soc.* **2008**, *130*, 9037–9047; c) E. Skulason, T. Bligaard, S. Gudmundsdóttir, F. Studt, J. Rossmeisl, F. Abild-Pedersen, T. Vegge, H. Jonsson, J. K. Nørskov, *Phys. Chem. Chem. Phys.* **2012**, *14*, 1235–1245.

[6] F. Zhou, L. M. Azofra, M. Ali, M. Kar, A. N. Simonov, C. McDonnell-Worth, C. Sun, X. Zhang, D. R. MacFarlane, *Energy Environ. Sci.* **2017**, *10*, 2516–2520.

[7] a) V. Kordali, G. Kyriacou, C. Lambrou, *Chem. Commun.* **2000**, *17*, 1673–1674; b) Z. Geng, Y. Liu, X. Kong, P. Li, K. Li, Z. Liu, J. Du, M. Shu, R. Si, J. Zeng, *Adv. Mater.* **2018**, *30*, 1803498; c) B. Yu, H. Li, J. White, S. Donne, J. Yi, S. Xi, Y. Fu, G. Henkelman, H. Yu, Z. Chen, *Adv. Funct. Mater.* **2020**, *30*, 1905665.

[8] G. Qing, R. Ghazfar, S. T. Jackowski, F. Habibzadeh, M. M. Ashtiani, C. P. Chen, M. R. Smith, 3rd, T. W. Hamann, *Chem. Rev.* **2020**, *120*, 5437–5516.

[9] L. Zhang, G. F. Chen, L. X. Ding, H. Wang, *Chem. Eur. J.* **2019**, *25*, 12464–12485.

[10] Z. Yao, Z. Nie, H. Yang, X. Zhou, Z. Liu, S. Huang, *Chem. Commun.* **2012**, *48*, 1027–1029.

[11] J. Wang, L. Yu, L. Hu, G. Chen, H. Xin, X. Feng, *Nat. Commun.* **2018**, *9*, 1–7.

[12] C. Lv, C. Yan, G. Chen, Y. Ding, J. Sun, Y. Zhou, G. Yu, *Angew. Chem. Int. Ed.* **2018**, *130*, 6181–6184.

[13] L. Zhang, L. X. Ding, G. F. Chen, X. Yang, H. Wang, *Angew. Chem. Int. Ed.* **2019**, *131*, 2638–2642.

[14] L. Zhang, X. Ji, X. Ren, Y. Ma, X. Shi, Z. Tian, A. M. Asiri, L. Chen, B. Tang, X. Sun, *Adv. Mater.* **2018**, *30*, 1800191.

[15] G.-F. Chen, X. Cao, S. Wu, X. Zeng, L.-X. Ding, M. Zhu, H. Wang, *J. Am. Chem. Soc.* **2017**, *139*, 9771–9774.

[16] a) P. Li, Z. Yang, J. Shen, H. Nie, Q. Cai, L. Li, M. Ge, C. Gu, X. Chen, K. Yang, L. Zhang, Y. Chen, S. Huang, *ACS Appl. Mater. Interfaces* **2016**, *8*, 3543–3550; b) J. Shen, Z. Yang, M. Ge, P. Li, H. Nie, Q. Cai, C. Gu, K. Yang, S. Huang, *ACS Appl. Mater. Interfaces* **2016**, *8*, 17284–17291.

[17] a) J. Xu, I. Amorim, Y. Li, J. Li, Z. Yu, B. Zhang, A. Araujo, N. Zhang, L. Liu, *Carbon Energy* doi.org/10.1002/cey1002.1056; b) J. Yang, Z. Yang, L. H. Li, Q. Cai, H. Nie, M. Ge, X. Chen, Y. Chen, S. Huang, *Nanoscale* **2017**, *9*, 6886–6894.

[18] X. Cui, C. Tang, Q. Zhang, *Adv. Energy Mater.* **2018**, *8*, 1800369.

[19] I. A. Amar, R. Lan, C. T. Petit, S. Tao, *J. Solid State Electrochem.* **2011**, *15*, 1845.

[20] H. Wang, L. Wang, Q. Wang, S. Ye, W. Sun, Y. Shao, Z. Jiang, Q. Qiao, Y. Zhu, P. Song, *Angew. Chem. Int. Ed.* **2018**, *57*, 12360–12364.

[21] a) M. M. Shi, D. Bao, S. J. Li, B. R. Wulan, J. M. Yan, Q. Jiang, *Adv. Energy Mater.* **2018**, *8*, 1800124; b) W. Xu, G. Fan, J. Chen, J. Li, L. Zhang, S. Zhu, X. Su, F. Cheng, J. Chen, *Angew. Chem. Int. Ed.* **2020**, *132*, 3539–3544.

[22] A. Essalik, K. Amouzegar, O. Savadogo, *J. Appl. Electrochem.* **1995**, *25*, 404–407.

[23] a) J. M. McEnaney, A. R. Singh, J. A. Schwalbe, J. Kibsgaard, J. C. Lin, M. Cargnello, T. F. Jaramillo, J. K. Nørskov, *Energy Environ. Sci.* **2017**, *10*, 1621–1630; b) K. Kim, C.-Y. Yoo, J.-N. Kim, H. C. Yoon, J.-I. Han, *J. Electrochem. Soc.* **2016**, *163*, F1523-F1526.

[24] Y. Huang, D. D. Babu, Z. Peng, Y. Wang, *Adv. Sci.* **2020**, *7*, 1902390.

[25] a) R. Zhao, H. Xie, L. Chang, X. Zhang, X. Zhu, X. Tong, T. Wang, Y. Luo, P. Wei, Z. Wang, X. Sun, *J. Energy Chem.* **2019**, *1*, 100011; b) X. Yan, D. Liu, H. Cao, F. Hou, J. Liang, S. X. Dou, *Small Methods* **2019**, *3*, 1800501.

[26] Y. Abghoui, E. Skúlason, *Catal. Today* **2017**, *286*, 69–77.

[27] M.-A. Légaré, G. Bélanger-Chabot, R. D. Dewhurst, E. Welz, I. Krummenacher, B. Engels, H. Braunschweig, *Science* **2018**, *359*, 896–900.

[28] a) Y. Zhan, Y. Li, Z. Yang, X. Wu, M. Ge, X. Zhou, J. Hou, X. Zheng, Y. Lai, R. Pang, H. Duan, H. Chen, H. Nie, S. Huang, *Adv. Sci.* **2019**, *6*, 1801663; b) Y. Zhan, X. Zhou, H. Nie, X. Xu, X. Zheng, J. Hou, H. Duan, S. Huang, Z. Yang, *J. Mater. Chem. A* **2019**, *7*, 15599–15606; c) X. Zheng, H. Nie, Y. Zhan, X. Zhou, H. Duan, Z. Yang, *J. Mater. Chem. A* **2020**, *8*, 8273–8280.

[29] a) T. Chen, S. Liu, H. Ying, Z. Li, J. Hao, *Chem. Asian J.* **2020**, *15*, 1081–1087; b) Y.-J. Mao, L. Wei, X.-S. Zhao, Y.-S. Wei, J.-W. Li, T. Sheng, F.-C. Zhu, N. Tian, Z.-Y. Zhou, S.-G. Sun, *Chem. Commun.* **2019**, *55*, 9335–9338; c) K. Kugler, M. Luhn, J. A. Schramm, K. Rahimi, M. Wessling, *Phys. Chem. Chem. Phys.* **2015**, *17*, 3768–3782.

[30] X. Liu, Y. Jiao, Y. Zheng, M. Jaroniec, S.-Z. Qiao, *J. Am. Chem. Soc.* **2019**, *141*, 9664–9672.

[31] H.-M. Liu, S.-H. Han, Y. Zhao, Y.-Y. Zhu, X.-L. Tian, J.-H. Zeng, J.-X. Jiang, B. Y. Xia, Y. Chen, *J. Mater. Chem. A* **2018**, *6*, 3211–3217.

[32] Z. Yang, X. Zhou, Z. Jin, Z. Liu, H. Nie, X. A. Chen, S. Huang, *Adv. Mater.* **2014**, *26*, 3156–3161.

[33] Y. Yao, H. Wang, X.-z. Yuan, H. Li, M. Shao, *ACS Energy Lett.* **2019**, *4*, 1336–1341.

[34] Y. Yao, S. Zhu, H. Wang, H. Li, M. Shao, *Angew. Chem. Int. Ed.* **2020**, *59*, 10479–10483.

[35] E. Tayyebi, Y. Abghoui, E. Skulason, *ACS Catal.* **2019**, *9*, 11137–11145.

[36] G. Deng, T. Wang, A. A. Alshehri, K. A. Alzahrani, Y. Wang, H. Ye, Y. Luo, X. Sun, *J. Mater. Chem. A* **2019**, *7*, 21674–21677.

[37] R. Manjunatha, A. Schechter, *Electrochem. Commun.* **2018**, *90*, 96–100.

[38] H. Wang, Y. Li, C. Li, K. Deng, Z. Wang, Y. Xu, X. Li, H. Xue, L. Wang, *J. Mater. Chem. A* **2019**, *7*, 801–805.

[39] H. Wang, Y. Li, D. Yang, X. Qian, Z. Wang, Y. Xu, X. Li, H. Xue, L. Wang, *Nanoscale* **2019**, *11*, 5499–5505.

[40] Z. Wang, C. Li, K. Deng, Y. Xu, H. Xue, X. Li, L. Wang, H. Wang, *ACS Sustainable Chem. Eng.* **2018**, *7*, 2400–2405.

[41] a) F. Pang, Z. Wang, K. Zhang, J. He, W. Zhang, C. Guo, Y. Ding, *Nano Energy* **2019**, *58*, 834–841; b) J. Bai, H. Huang, F.-M. Li, Y. Zhao, P. Chen, P.-J. Jin, S.-N. Li, H.-C. Yao, J.-H. Zeng, Y. Chen, *J. Mater. Chem. A* **2019**, *7*, 21149–21156; c) C. Chen, Y. Chen, A. M. Ali, W. Luo, J. Wen, L. Zhang, H. Zhang, *Chem. Eng. Technol.* **2020**, *43*, 719–730.

[42] a) D. Chen, Y. Wang, D. Liu, H. Liu, C. Qian, H. He, J. Yang, *Carbon Energy* doi.org/10.1002/cey1002.1038; b) L. Chai, Z. Hu, X. Wang, Y. Xu, L. Zhang, T. T. Li, Y. Hu, J. Qian, S. Huang, *Adv. Sci.* **2020**, *7*, 1903195.

[43] H. Zhao, D. Zhang, Z. Wang, Y. Han, X. Sun, H. Li, X. Wu, Y. Pan, Y. Qin, S. Lin, *Appl. Catal. B* **2020**, *265*, 118481.

[44] M. Ma, X. Han, H. Li, X. Zhang, Z. Zheng, L. Zhou, J. Zheng, Z. Xie, Q. Kuang, L. Zheng, *Appl. Catal. B* **2020**, *265*, 118568.

[45] W. Tong, B. Huang, P. Wang, L. Li, Q. Shao, X. Huang, *Angew. Chem. Int. Ed.* **2020**, *59*, 2649–2653.

[46] a) C. Hu, X. Chen, J. Jin, Y. Han, S. Chen, H. Ju, J. Cai, Y. Qiu, C. Gao, C. Wang, *J. Am. Chem. Soc.* **2019**, *141*, 7807–7814; b) Z. Sun, X. Wang, H. Zhao, S. W. Koh, J. Ge, Y. Zhao, P. Gao, G. Wang, H. Li, *Carbon Energy* **2020**, *2*, 122–130; c) J. Lv, Z. Tian, K. Dai, Y. Ye, C. Liang, *J. Colloid Interface Sci.* **2019**, *553*, 126–135.

[47] R. D. Kumar, Z. Wang, C. Li, A. V. N. Kumar, H. Xue, Y. Xu, X. Li, L. Wang, H. Wang, *J. Mater. Chem. A* **2019**, *7*, 3190–3196.

[48] a) Z. Yang, X. Zhou, H. Nie, Z. Yao, S. Huang, *ACS Appl. Mater. Interfaces* **2011**, *3*, 2601–2606; b) X. Zhou, Z. Tian, J. Li, H. Ruan, Y. Ma, Z. Yang, Y. Qu, *Nanoscale* **2014**, *6*, 2603–2607; c) H. Wei, Q. Xi, X. A. Chen, D. Guo, F. Ding, Z. Yang, S. Wang, J. Li, S. Huang, *Adv. Sci.* **2018**, *5*, 1700733.

[49] J. Lv, S. Wu, Z. Tian, Y. Ye, J. Liu, C. Liang, *J. Mater. Chem. A* **2019**, *7*, 12627–12634.

[50] B. H. Suryanto, D. Wang, L. M. Azofra, M. Harb, L. Cavallo, R. Jalili, D. R. Mitchell, M. Chatti, D. R. MacFarlane, *ACS Energy Lett.* **2018**, *4*, 430–435.

[51] a) X. Zhou, Z. Yang, H. Nie, Z. Yao, L. Zhang, S. Huang, *J. Power Sources* **2011**, *196*, 9970–9974; b) Z. Liu, H. Nie, Z. Yang, J. Zhang, Z. Jin, Y. Lu, Z. Xiao, S. Huang, *Nanoscale* **2013**, *5*, 3283–3288; c) J. Su, H. Zhao, W. Fu, W. Tian, X. Yang, H. Zhang, Y. Wang, *Appl. Catal. B* **2020**, *265*, 118589.

[52] H. Wang, D. Yang, S. Liu, S. Yin, Y. Xu, X. Li, Z. Wang, L. Wang, *ACS Sustainable Chem. Eng.* **2019**, *7*, 15772–15777.

[53] a) Z. Yang, Z. Yao, G. Li, G. Fang, H. Nie, Z. Liu, X. Zhou, X. A. Chen, S. Huang, *ACS Nano* **2012**, *6*, 205–211; b) Z. Jin, H. Nie, Z. Yang, J. Zhang, Z. Liu, X. Xu, S. Huang, *Nanoscale* **2012**, *4*, 6455–6460.

[54] J. Wang, B. Huang, Y. Ji, M. Sun, T. Wu, R. Yin, X. Zhu, Y. Li, Q. Shao, X. Huang, *Adv. Mater.* **2020**, *32*, 1907112.

[55] Y. Yang, X.-X. Xue, Q.-j. Chen, Y. Feng, *J. Chem. Phys.* **2019**, *151*, 144710.

[56] H. K. Lee, C. S. L. Koh, Y. H. Lee, C. Liu, I. Y. Phang, X. Han, C.-K. Tsung, X. Y. Ling, *Sci. Adv.* **2018**, *4*, eaar3208.

[57] Y.-C. Hao, Y. Guo, L.-W. Chen, M. Shu, X.-Y. Wang, T.-A. Bu, W.-Y. Gao, N. Zhang, X. Su, X. Feng, *Nat. Catal.* **2019**, *2*, 448–456.